AGU PUBLICATIONS

JGR

Journal of Geophysical Research: Atmospheres

RESEARCH ARTICLE
10.1002/2016JD025363

Key Points:
- The assimilation of DYNAMO observations improves the vertical profiles of GEOS-5 reanalysis temperature and moisture over the DYNAMO region
- The assimilation of DYNAMO observations produces stronger local westerly acceleration and zonal wind shear in the GEOS-5 reanalysis
- The assimilation of DYNAMO observations improves the GEOS-5 reanalysis representation of MJO initiation processes

Correspondence to:
D. Achuthavarier,
deepthi.achuthavarier@nasa.gov

Citation:
Achuthavarier, D., H. Wang, S. D. Schubert, and M. Sienkiewicz (2017), Impact of DYNAMO observations on NASA GEOS-5 reanalyses and the representation of MJO initiation, *J. Geophys. Res. Atmos.*, *122*, 179–201, doi:10.1002/2016JD025363.

Received 13 MAY 2016
Accepted 16 DEC 2016
Accepted article online 17 DEC 2016
Published online 11 JAN 2017

Impact of DYNAMO observations on NASA GEOS-5 reanalyses and the representation of MJO initiation

D. Achuthavarier[1,2], H. Wang[1,3], S. D. Schubert[1], and M. Sienkiewicz[1,3]

[1]Global Modeling and Assimilation Office, NASA GSFC, Greenbelt, Maryland, USA, [2]Universities Space Research Association, Columbia, Maryland, USA, [3]Science Systems and Applications, Inc, Lanham, Maryland, USA

Abstract This study examines the impact of the Dynamics of the Madden-Julian Oscillation (DYNAMO) campaign in situ observations on NASA Goddard Earth Observing System version 5 (GEOS-5) reanalyses and the improvements gained thereby in the representation of the Madden-Julian Oscillation (MJO) initiation processes. To this end, we produced a global, high-resolution (1/4° spatially) reanalysis that assimilates the level-4, quality-controlled DYNAMO upper air soundings from about 87 stations in the equatorial Indian Ocean region along with a companion data-denied control reanalysis. The DYNAMO reanalysis produces a more realistic vertical structure of the temperature and moisture in the central tropical Indian Ocean by correcting the model biases, namely, the cold and dry biases in the lower troposphere and warm bias in the upper troposphere. The reanalysis horizontal winds are substantially improved, in that, the westerly acceleration and vertical shear of the zonal wind are enhanced. The DYNAMO reanalysis shows enhanced low-level diabatic heating, moisture anomalies and vertical velocity during the MJO initiation. Due to the warmer lower troposphere, the deep convection is invigorated, which is evident in convective cloud fraction. The GEOS-5 atmospheric general circulation model (AGCM) employed in the reanalysis is overall successful in assimilating the additional DYNAMO observations, except for an erroneous model response for medium rain rates, between 700 and 600 hPa, reminiscent of a bias in earlier versions of the AGCM. The moist heating profile shows a sharp decrease there due to the excessive convective rain re-evaporation, which is partly offset by the temperature increment produced by the analysis.

1. Introduction

The Madden-Julian Oscillation (MJO) is the dominant mode of subseasonal variability in the tropics with a periodicity of 30–60 days, which is characterized by an eastward propagation of convection and associated circulation anomalies at an average speed of 5 m s^{-1} [*Madden and Julian*, 1971, 1972]. The convective signal of the MJO typically first forms in the central equatorial Indian Ocean and propagates eastward, accompanied by circulation anomalies in the form of Rossby and Kelvin waves, forming a global circumnavigating signal along the equator. The MJO has widespread impacts on the global weather and climate and is considered a major source of global predictability on subseasonal time scales [*Zhang*, 2005; *Waliser*, 2011; *Zhang et al.*, 2013]. While substantial progress has been made in understanding the salient features of the MJO [e.g., *Wang*, 2011], considerable challenges remain in understanding the physical processes as well as simulating and predicting the MJO in current general circulation models, particularly its initiation over the tropical Indian Ocean [*Lin et al.*, 2006; *Seo et al.*, 2009; *Kim et al.*, 2010; *Hung et al.*, 2013].

State-of-the-art global reanalyses are among the most widely used data sets to study the MJO. While these reanalysis products provide a large-scale view of MJO processes and have produced a credible representation of the MJO signature [e.g., *Robertson and Roberts*, 2012], their quality in representing the observed physical processes associated with the MJO is often questionable. For example, recent reanalyses show varying estimates of the evolution of the vertical heating profile throughout the life cycle of the MJO, particularly over the tropical Indian Ocean [*Ling and Zhang*, 2011; *Jiang et al.*, 2011]. Such variations in reanalyses are largely due to poor in situ data networks in the tropics, especially in the tropical Indian Ocean, where the reanalyses are mostly constrained by satellite observations which have relatively poor vertical resolution; their vertical profiles thus are strongly subject to the deficiencies in the assimilating atmospheric general circulation models (AGCMs) used. It is thus imperative to have more in situ observations over the tropical Indian

Ocean to better understand the physical processes associated with MJO initiation, to evaluate reanalyses, and to identify physical deficiencies in current AGCMs.

The Dynamics of the MJO (DYNAMO) field experiment was conducted in the tropical Indian Ocean during 1 October 2011 to 31 March 2012, under the Cooperative Indian Ocean Experiment on Intraseasonal Variability in the Year 2011, with a specific objective of advancing our understanding of the initiation mechanisms of the MJO [*Yoneyama et al*., 2013]. An important and primary component of this project was to collect high-quality observations from the equatorial Indian Ocean region where the genesis of the MJO takes place and to facilitate its integration into other aspects such as modeling, data analysis, and real-time forecasting. The DYNAMO collected atmospheric and oceanic observations from a number of instrument platforms, including radiosondes, aircraft, radars, wind profilers, and satellites. During the DYNAMO period, three MJO events developed in the vicinity of the sounding network, providing an unprecedented wealth of data, prior to, during, and after those events in the central tropical Indian Ocean, an otherwise data sparse area.

Despite the large volume of satellite data, the conventional in situ observations remain an important component in the analysis, as can be seen on the NASA Global Modeling and Assimilation Office (GMAO)'s observation-impact-monitoring page (https://gmao.gsfc.nasa.gov/forecasts/systems/fp/obs_impact/) [*Gelaro et al*., 2010]. The in situ observations from the DYNAMO field campaign provide us with an excellent and unique opportunity to assess its impact on the overall quality of NASA GMAO analyses, and in particular the representation in GMAO reanalyses of the MJO initiation processes over the tropical Indian Ocean. In this paper, we present a high-resolution, global reanalysis, referred to as the DYNAMO reanalysis, produced by assimilating the quality-controlled and spatially complete DYNAMO observations, particularly the upper air soundings, in a recent version of the NASA GMAO atmospheric data assimilation system. We note that although most of the DYNAMO observations are made available to the operational weather centers via global telecommunication system (GTS) [*Yoneyama et al*., 2013], high vertical resolution, spatially complete and quality-controlled data are assimilated neither in the real-time analyses nor in the retrospective reanalyses. The DYNAMO reanalysis presented here is an attempt to provide a comprehensive global reanalysis for the DYNAMO period. Along with the DYNAMO reanalysis, a companion control reanalysis is produced where the DYNAMO observations are withheld. The DYNAMO and the control reanalyses together form unique data sets that enable us to investigate the impact of in situ observations over the tropical Indian Ocean in the GMAO reanalysis system with a focus on the representation of the known MJO initiation processes. Here we note that the focus is not as much on finding new initiation mechanisms but on developing an improved reanalysis that would facilitate that.

Section 2 provides details of the assimilated DYNAMO observations, the NASA Goddard Earth Observing System version 5 (GEOS-5) data assimilation system and on the design of the control and the DYNAMO reanalyses. The impact of the DYNAMO observations in the GEOS-5 analysis system from the assimilation point of view is presented in section 3. The impact of the DYNAMO observations on the representation of the MJO is discussed in section 4. Section 5 briefly discusses the critical role of the model physics in the reanalysis system, and section 6 provides summary.

2. Data and Experiments

2.1. DYNAMO Observations

The DYNAMO observations assimilated in the DYNAMO reanalysis are the level-4 (L4) quality-controlled, 6-hourly or more frequent, upper air soundings described in *Ciesielski et al.* [2014], which are obtained from the online DYNAMO data archive at the National Center for Atmospheric Research Earth Observing Laboratory (http://data.eol.ucar.edu/codiac/ds_proj?DYNAMO). The L4 data consist of 5 hPa uniform vertical resolution profiles derived from the original high vertical resolution (5–10 m) data, wherever available, as well as the GTS-resolution data for a number of priority and nonpriority sounding sites. Both have undergone quality checks. As discussed in *Ciesielski et al.* [2014], a number of errors, such as daytime dry bias, errors in baseline surface data, ship deck heating effects, and artificial dry spikes in slow-ascent sondes, were corrected in producing the L4 observations. We note that the L4 data are more comprehensive and of higher quality compared to the real-time transmissions of the DYNAMO observations through the World Meteorological Organization's GTS network (referred to as GTS data, hereafter) that were assimilated in routine weather analyses at many global weather analysis centers. The GTS data contain relatively fewer vertical levels, with approximately 15–25 hPa vertical resolution.

Table 1. Various Upper Air Soundings Sources, Their Vertical Resolution and the Number of Stations in Each Category That Are Assimilated in the DYNAMO Reanalysis[a]

Site Type	Vertical Resolution	Number of Sites
Enhanced stations	5 hPa	7
Ships	5 hPa	4
PSS (high-resolution)	5 hpa	21
Dropsonde	5 hPa	1
PSS (low-resolution)	GTS	17
NPSS	GTS	10
Pibal (winds only)	GTS	27
Total		87

[a]Temperature and humidity from seven low-resolution PSS and six NPSS are not assimilated due to historically poor data quality from those stations. The number of low-resolution PSS and NPPS listed here excludes those stations.

Observations from a total of 87 stations (Table 1), which span over the Indian Ocean and the maritime continent from 30°E–150°E, 20°S–20°N, are utilized in this study. The majority of the observations fall within 1 October 2011 to 31 March 2012, except for the Gan Island, where 1200 UTC data begin on 1 September 2011 and extend through 8 April 2012. The sounding network in the central tropical Indian Ocean consists of the enhanced observing sites in Diego Garcia, Gan, Malé, and Colombo as well as the research vessels that were stationed adjacent to those, forming the two quadrilateral sounding arrays. In addition, data from several routine weather stations in the region that were designated as priority or the nonpriority sites, pibal profiles from several Indonesian stations, and dropsonde data from the NOAA P-3 aircraft based in Diego Garcia are assimilated. The NOAA P-3 had 12 missions from 9 November 9 to 13 December 2011. Among the priority sounding sites, 21 stations have 5 hPa vertical resolution data whereas the remaining 17 have GTS-resolution data (15–25 hPa).

The 87 stations mentioned above exclude seven priority and six nonpriority sounding sites that have historically poor-quality temperature and humidity data, which are typically not assimilated in the GEOS-5 analysis. However, horizontal winds from these stations are assimilated. Humidity and temperature from the 5 hPa vertical resolution data are assimilated wherever available. In its absence, data of GTS vertical resolution are assimilated. All data, regardless of the vertical resolution, are from the L4 quality-controlled collection. The variables assimilated are horizontal winds, temperature, specific humidity, and surface pressure, except for pibal profiles, where only horizontal winds are recorded. The pibal observations are generally made at 0600 and 1800 UTC between the radiosonde recordings at 0000 and 12000 UTC and mostly for the lowest few kilometers of the troposphere.

2.2. Assimilation System

The DYNAMO observations are assimilated using a recent version of the NASA GMAO atmospheric data assimilation system (ADAS), which consists of the Goddard Earth Observing System version 5 (GEOS-5) AGCM [*Rienecker et al.*, 2008; *Molod et al.*, 2015] along with the Grid point Statistical Interpolation (GSI) analysis [*Wu et al.*, 2002; *Kleist et al.*, 2009], which is jointly developed by the GMAO and the National Centers for Environmental Prediction. Specifically, the GEOS-5 ADAS has the internal designation 5.12.4 (tagged on 4 April 2014), while the GEOS-5 AGCM is Ganymed-4.0.beta10, (tagged on 13 March 2014).

The GEOS-5 AGCM consists of a finite volume dynamical core [*Lin*, 2004], various physics packages and the catchment land surface model [*Koster et al.*, 2000], all integrated by the Earth System Modeling Framework. The AGCM has 72 hybrid levels in the vertical and employs a cubed sphere grid in the horizontal [*Putman and Lin*, 2007], which provides improved uniformity in grid spacing and avoids grid spacing singularities that is often found in latitude-longitude grids. The model physics includes a modified form of the Relaxed Arakawa-Schubert scheme [*Moorthi and Suarez*, 1992] with a stochastic Tokioka trigger function for deep convection, improved moist physics and prognostic cloud microphysics as described in *Bacmeister et al.* [2006], Monin-Obukhov surface layer parameterization that takes into account the effects of a viscous sublayer for heat and moisture transport [*Helfand and Schubert*, 1995], and turbulence schemes by *Lock et al.* [2000] and *Louis et al.* [1982]. A detailed account of the most recent updates in the AGCM physics package can be found in *Molod et al.* [2015], which include, for instance, increased re-evaporation of frozen precipitation and cloud condensate and improved representation of gravity wave drag.

The GSI analysis is a three-dimensional variational algorithm with a 6 h update cycle along with the incremental analysis update (IAU) procedure by *Bloom et al.* [1996]. The IAU approach, in which the analysis corrections are added in the model equations incrementally through an additional tendency term, minimizes the sudden perturbations that can occur when the analysis is introduced to the model background.

The observing system used in the control and the DYNAMO reanalyses consists of conventional in situ upper air data, satellite radiance, satellite retrievals, and land and ocean surface observations. The conventional observations consist of upper air data from radiosondes, pibal, wind profilers, aircraft reports, and dropsondes. Other observations include Next Generation Radar winds, Tropical Rainfall Measuring Mission (TRMM) Microwave Imager (TMI) rain rates, and cloud top winds from various satellites. Surface observations from land stations as well as ships and buoys are assimilated. Other key observation platforms include Global Positioning System radio occultation, Atmospheric Infrared Sounder (AIRS), and hyperspectral Infrared Atmospheric Sounding Interferometer (IASI). The sea surface temperature is the daily data of 1/20° horizontal resolution from the Operational Sea Surface Temperature and Sea Ice Analysis [*Donlon et al*., 2012].

2.3. DYNAMO and Control Reanalyses

The DYNAMO reanalysis and its companion control reanalysis are produced at 1/4 degree horizontal resolution (0.25° × 0.3125°) with the GSI analysis computed in a 1/2° grid (0.5° × 0.625°). Both reanalyses are initialized on 31 May 2011, 2100 UTC from the GMAO operational analysis fields, and are run through 30 June 2012, producing output for a total of 13 months.

To illustrate the spatial and temporal distribution of the DYNAMO observations in the DYNAMO reanalysis, radiosonde specific humidity data counts are shown in Figure 1, as an example. Figure 1a shows mean radiosonde specific humidity data counts for all vertical levels combined for the period 1 October 2011 to 31 March 2012 for the DYNAMO and the control reanalyses. The DYNAMO observations, shaded in red, are centered in the tropical Indian Ocean and over the maritime continent. The spread around the two quadrilateral sounding arrays is due to the movement of research vessels in and out of the region. Particularly, the feature extending in the southwest Indian Ocean toward the Madagascar Island is from the data collected as the research vessel Revelle departed the site in February 2012. In contrast, the data withholding control reanalysis shows no sounding observations in the DYNAMO region. It should be noted that in the control reanalysis, all the DYNAMO GTS-resolution data that were transmitted to the GMAO routine conventional data buffer were removed so as to have a clean control experiment that provided maximum contrast with the DYNAMO reanalysis.

Figure 1b uses radiosonde specific humidity as an example to show the evolution of the DYNAMO observation data count in time, where the total data count in the DYNAMO region for all vertical levels combined builds up in early October 2011 and ceases by the end of March 2012.

We note that in comparison with the newly released GMAO reanalysis Modern-Era Retrospective analysis for Research and Applications, version 2 (MERRA-2) [*Bosilovich et al*., 2015], the DYNAMO reanalysis provides an upgraded reanalysis for the DYNAMO period, which has higher horizontal resolution (MERRA-2 is 1/2° spatially) and higher quality DYNAMO observations assimilated. In MERRA-2, only the real-time GTS submissions of the DYNAMO soundings are assimilated, which as mentioned earlier, are of relatively low vertical resolution (15–25 hPa),and devoid of the corrections discussed in *Ciesielski et al.* [2014]. These data also could be less comprehensive where not all stations are likely to have made to the GTS in time. The fact that MERRA-2 is of slightly coarser horizontal resolution alone can lead to considerable difference between the DYNAMO reanalysis and MERRA-2, especially in regions where convective processes are important, due to the resolution-dependent convective trigger function in the GEOS-5 model [*Molod et al*., 2015]. Figure 2 compares the difference between the DYNAMO and the control reanalyses against that between the DYNAMO and the MERRA-2 for the period 1 October to 30 November 2011 for zonal wind, temperature, and specific humidity at 750 hPa. We chose 750 hPa pressure level because that is where the difference between the DYNAMO and control reanalyses is maximum. (This will be later demonstrated in Figures 7b and 9a and 9b.) While the difference between the control and the DYNAMO reanalyses is mostly limited to the DYNAMO region, the difference with respect to MERRA-2 is spread over the tropical belt. Over the central tropical region, the DYNAMO-MERRA-2 panels do show slightly smaller amplitude compared to DYNAMO-control, suggesting a possible influence of GTS-

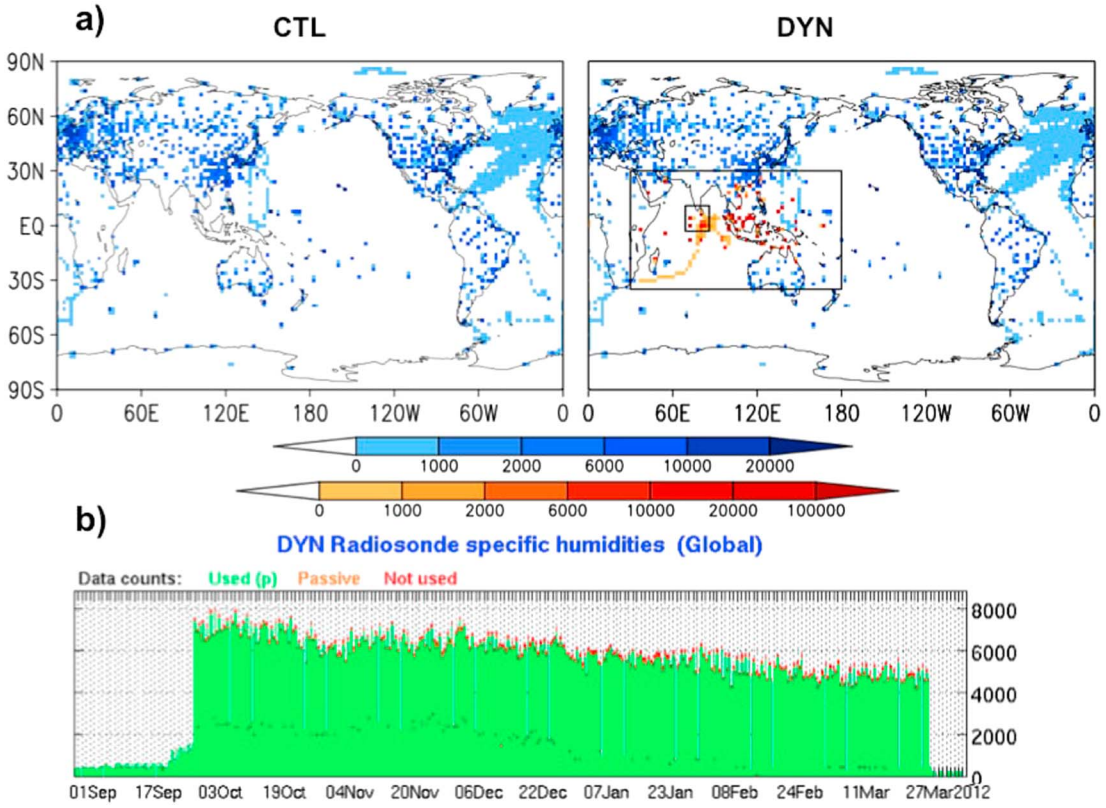

Figure 1. (a) Mean radiosonde specific humidity data counts for the 1 October 2011 to 31 March 2012 and all vertical pressure levels combined, for the control and the DYNAMO reanalyses. The red shading indicates DYNAMO stations and the blue the regular. In Figure 1a (right), the DYNAMO domain is indicated by large rectangle and the NSA by a small rectangle. (b) The bar chart showing number of DYNAMO radiosonde specific humidity observations for all vertical levels combined as a function of time, where green section represents used data, and yellow and red sections represent passive and rejected data, respectively. Both passive and rejected data are not used in the analysis.

resolution DYNAMO data in MERRA-2. Similar comparisons of monthly mean fields with reanalyses and operational analyses from other centers were also performed, but the differences in those cases were more dispersed and proved difficult to interpret due to the various differences in background model and assimilation algorithms (figure not shown). Therefore, a control reanalysis was deemed necessary to cleanly separate the impact of the DYNAMO observations. As such, in this study we focus on the difference between our control and DYNAMO reanalyses.

3. Impact of DYNAMO Observations in the GEOS-5 ADAS

In this study, we primarily focus our investigation on the DYNAMO Northern Sounding Array (NSA) region (70°E–85°E, 2°S–10°N) which covers the stations Gan, Malé, Colombo, and Revelle, mainly because the two MJOs observed during the DYNAMO period were more predominant there [*Yoneyama et al.*, 2013; *Johnson and Ciesielski*, 2013]. The overall impact of the DYNAMO data is largely limited within the DYNAMO region (as evident in Figure 2a) and is consistent with the assimilation experiments performed at the European Centre for Medium-Range Weather Forecasts (ECMWF) [*Ling et al.*, 2014]. This is clearly seen in Figures 2a–2c, where the differences are mostly within the DYNAMO region, except for moisture for which the model's response seems to have generated small differences over a larger region. Although the focus here is the NSA region, the impact over the greater DYNAMO region is largely in agreement with the results presented for the NSA region: we will briefly come back to this point later in the paper. We focus on 1 October to 31 December 2011, a period that has been extensively studied using DYNAMO observations [*Johnson and Ciesielski*, 2013; *Johnson et al.*, 2015; *Ruppert and Johnson*, 2015].

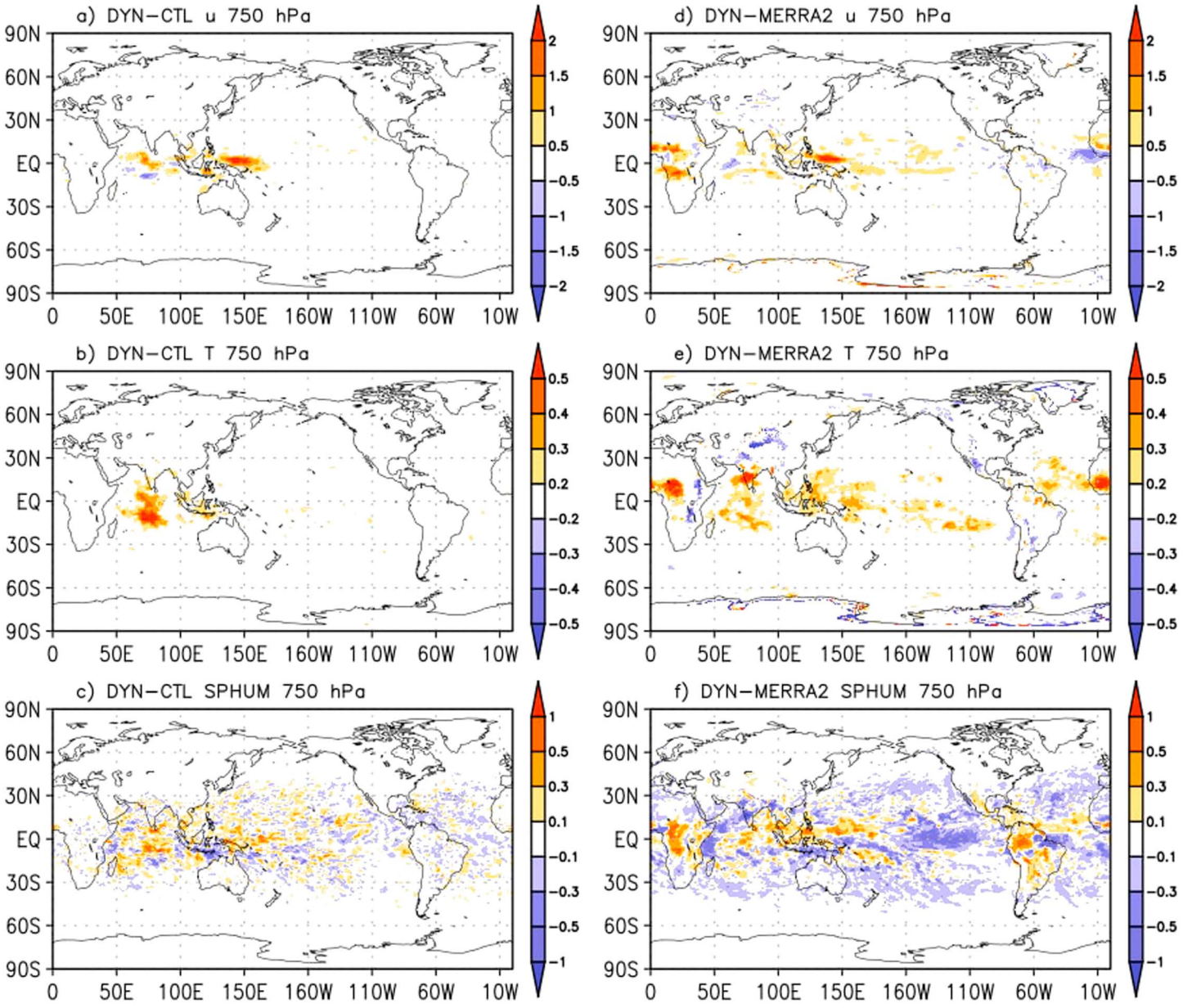

Figure 2. Difference between DYNAMO and control reanalyses and DYNAMO and MERRA-2 reanalyses for (a and d) zonal wind (m s^{-1}), (b and e) air temperature (K), and (c and f) specific humidity (g kg^{-1}) at 750 hPa. All fields are averaged from 1 October to 30 November 2011.

3.1. Analysis and Forecast Departures

The quality of the analysis and the impact of the observations are generally assessed by examining the departures between the model forecast (the first guess or the model background) and the observations (O-F), and those between the analysis and the observations (O-A). A successful analysis is marked by a notably smaller in magnitude O-A compared with O-F. We emphasize that here, the "observations" (O) represents DYNAMO observations alone and does not include other non-DYNAMO data, which allows us to cleanly examine the impact of DYNAMO observations. Also, since there are hardly any non-DYNAMO stations in the central tropical Indian Ocean, the region where the DYNAMO stations are located, an examination of O-A and O-F for the control reanalysis is irrelevant. Figure 3 shows the mean O-F and O-A for the DYNAMO observations of temperature, specific humidity, and horizontal winds, obtained as gridded products in pressure coordinates and averaged over the DYNAMO NSA region.

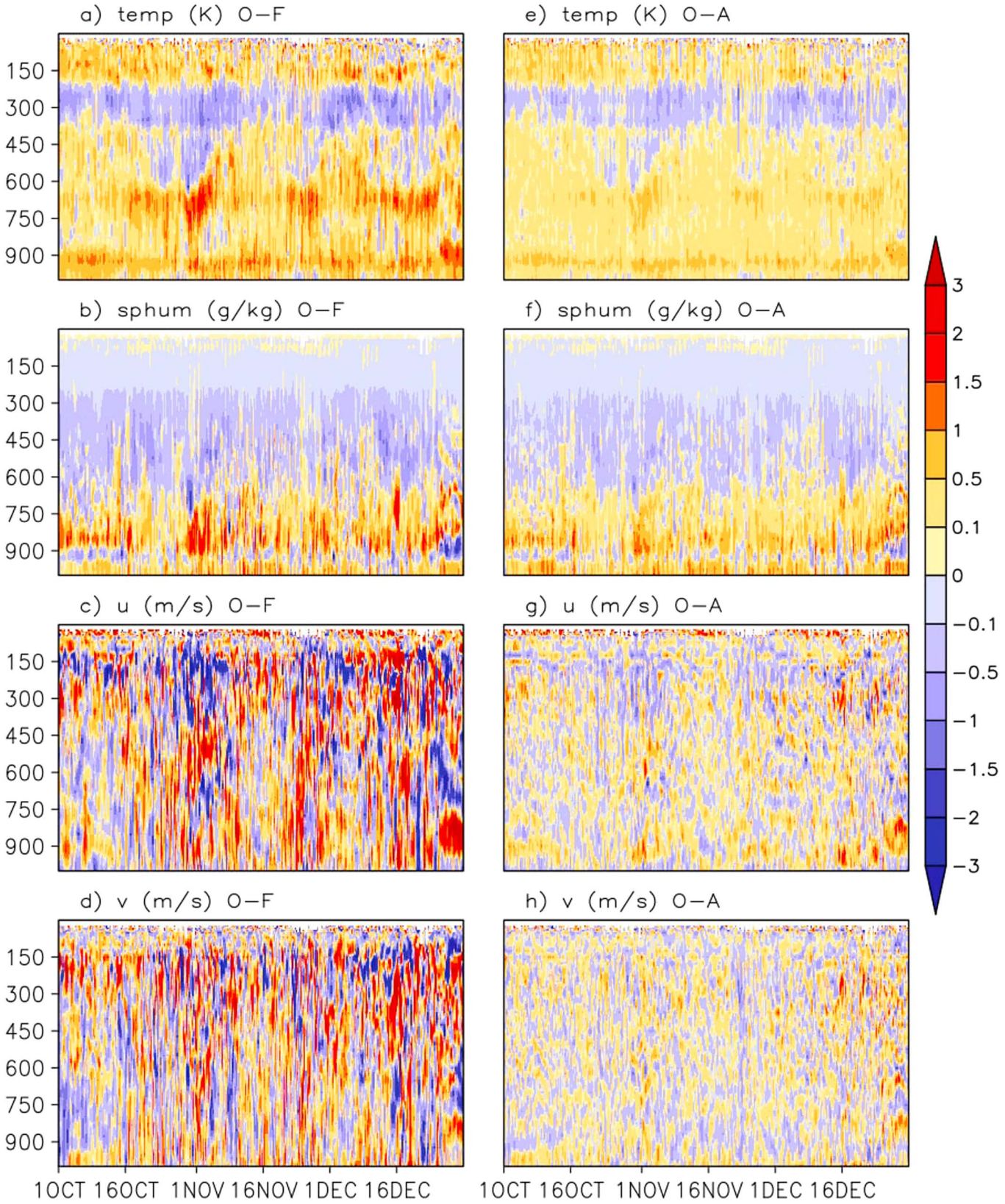

Figure 3. Mean (O-F) profiles of (a) temperature (K), (b) specific humidity (g kg^{-1}), (c) zonal and (d) meridional winds (m s^{-1}), averaged over the DYNAMO NSA, and (e–h) their corresponding (O-A) profiles. *Y* axis is pressure levels in hectopascals and *X* axis is time in days from 1 October to 31 December 2011. All data are from the DYNAMO reanalysis.

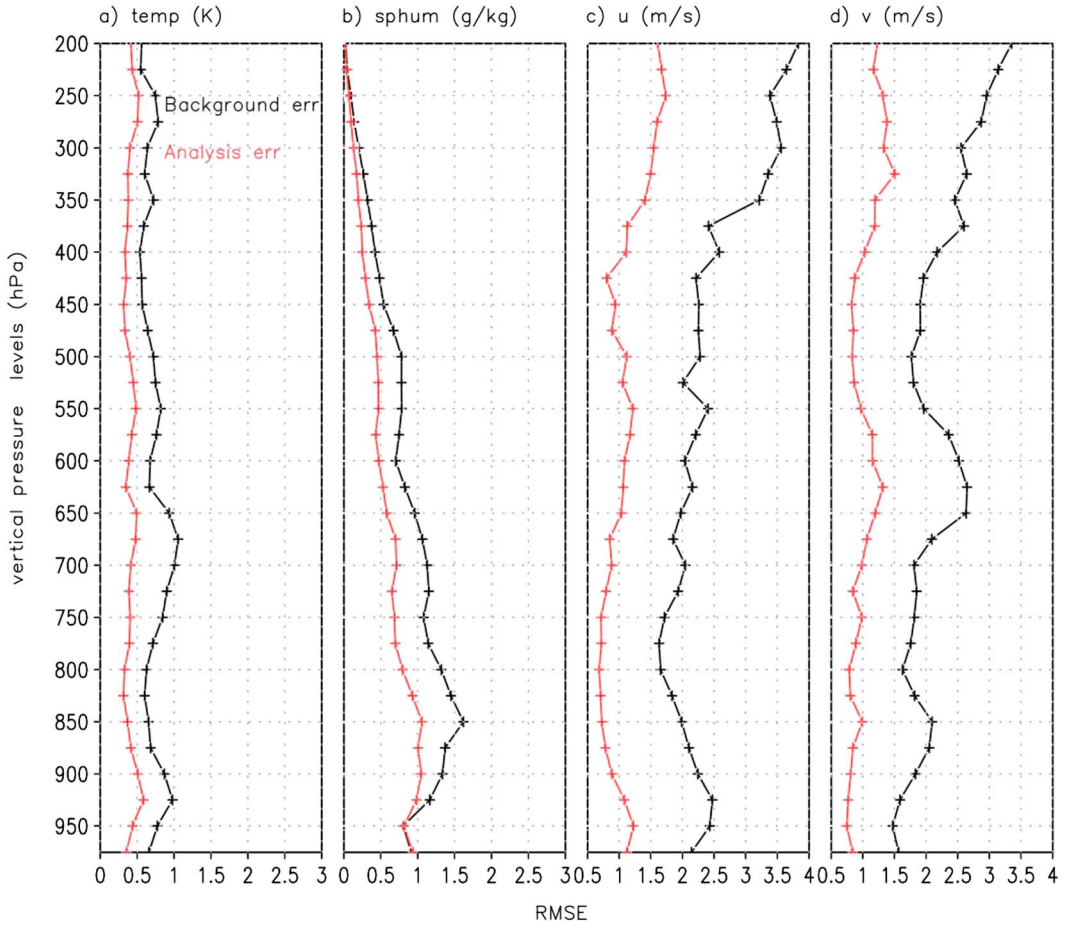

Figure 4. Vertical profiles of area-averaged root-mean-square error for background (black) and analysis (red) errors for DYNAMO observations in DYNAMO reanalysis. The averaging domain is DYNAMO NSA, and variables are (a) temperature (K), (b) specific humidity (g kg^{-1}), and (c) zonal and (d) meridional winds (m s^{-1}). *Y* axis is pressure levels in hectopascals. All data are from the DYNAMO reanalysis.

The assimilation of the DYNAMO observations corrects considerably the model biases in temperature and wind fields. (We note that the biases discussed here not necessarily represent characteristics of long-term climate biases in the GEOS-5 but are rather mean short-term tendencies that are partly corrected by the analysis increments during the assimilation process. Details of the mean climate biases in the AGCM can be found in *Molod et al*. [2015], where an evaluation of a 30 year long model simulation is presented.) The model cold bias in the lower troposphere extending from the surface to 600 hPa and warm bias aloft at about 300 hPa are notably reduced in the analysis, producing a vertical profile that is largely in agreement with the observations. The specific humidity observations attempt to reduce the model dry bias in the lower layers (surface—700 hPa). There is some indication of reduced wet bias between 600 and 400 hPa (Figures 3b and 3f), although the magnitude of correction is rather small. The corrections in the middle-upper troposphere are not as distinct as in the lower troposphere because of the inherently low specific humidity there, but even small corrections can be beneficial there since middle-upper level specific humidity is an important variable in determining the outgoing longwave radiation (OLR). The analysis draws largely from the winds than the temperature and moisture, and this is likely due to the larger background error variance of the wind fields. In the tropics, due to the relatively flat gradients, the temperature has smaller background error variance, one of the factors that determine how well the analysis draws to a quantity.

The root-mean-square (RMS) of O-F and O-A also show a consistent picture similar to the mean profiles discussed above. The RMS errors for four key quantities averaged over NSA and 1 October to 31 December 2011 show a notable reduction from background error to analysis error (Figure 4). Overall,

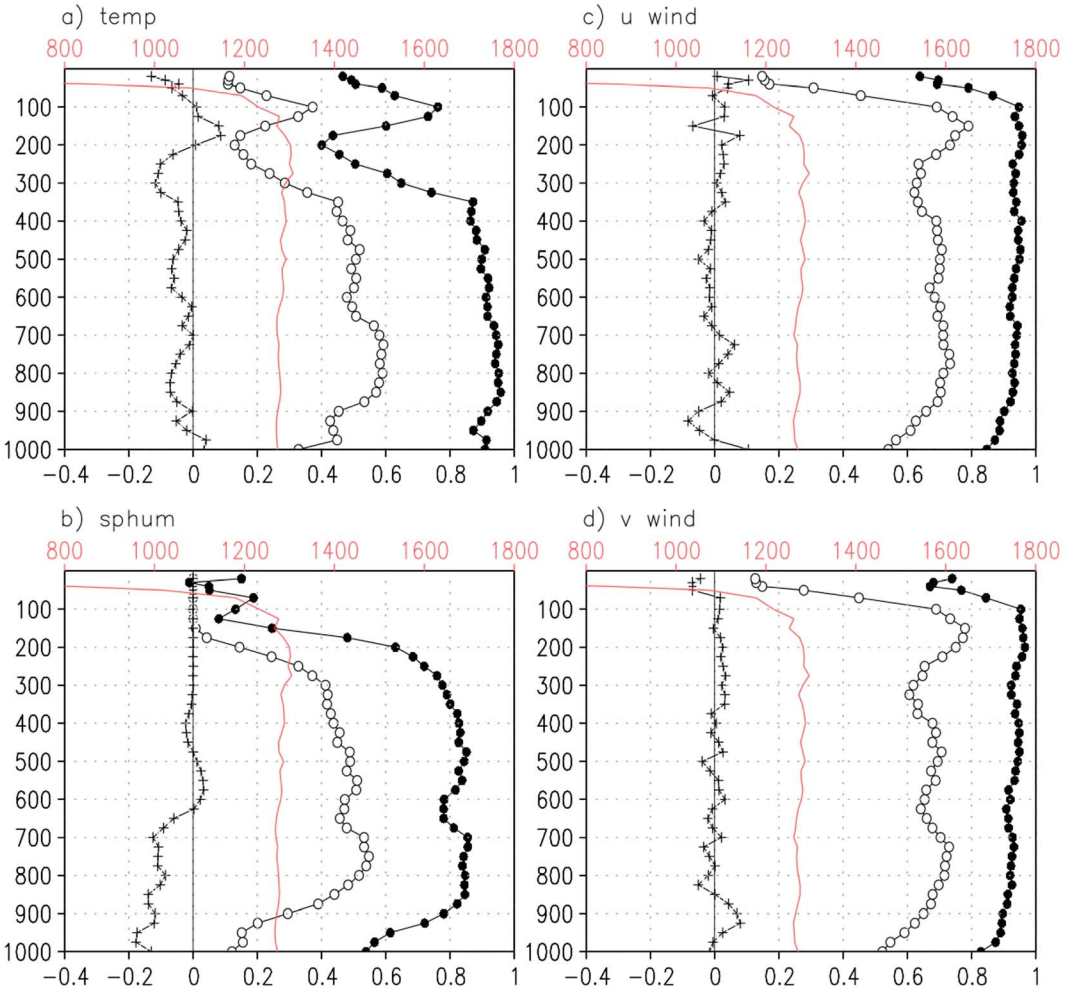

Figure 5. Vertical profiles of (open circles) effective gain, K, (plus sign) contextual bias, B, (closed circle) correlation between (O-F) and (A-F), and, (red solid line) total observation count for all DYNAMO radiosonde stations in the NSA domain for the period 1 October to 31 December 2011. Individual panels are for (a) temperature, (b) specific humidity, and (c) zonal wind and (d) meridional winds. Observation count is along the top *X* axis. *Y* axis is pressure in hectopascals.

Figures 3 and 4 provide a preliminary confirmation that the analyzed fields in the DYNAMO reanalysis are considerably drawn to the DYNAMO observations.

3.2. Effective Gain and Contextual Bias

The effective gain and contextual bias, originally proposed by A. Da Silva (personal communication, 2016) and further discussed in *Bosilovich and Da Silva* [2013], are useful metrics to further quantify the impact of specific observing systems on the analysis. They are derived using the O-F, which represents the error of the model forecast with respect to a single observing system (here the DYNAMO soundings), and the A-F, which stands for the collective final error after accounting for inputs from all observing systems, instruments, and background errors:

$$(A - F) = K \times (O - F) + B \tag{1}$$

In equation (1), *K* is the effective gain, which is a measure of how much the assimilation system has drawn to a particular observing system, and *B* is the contextual bias, which is a measure of the degree of agreement between a given observation type and all other observation types assimilated. Zero contextual bias suggests that there is no competition from other observing systems.

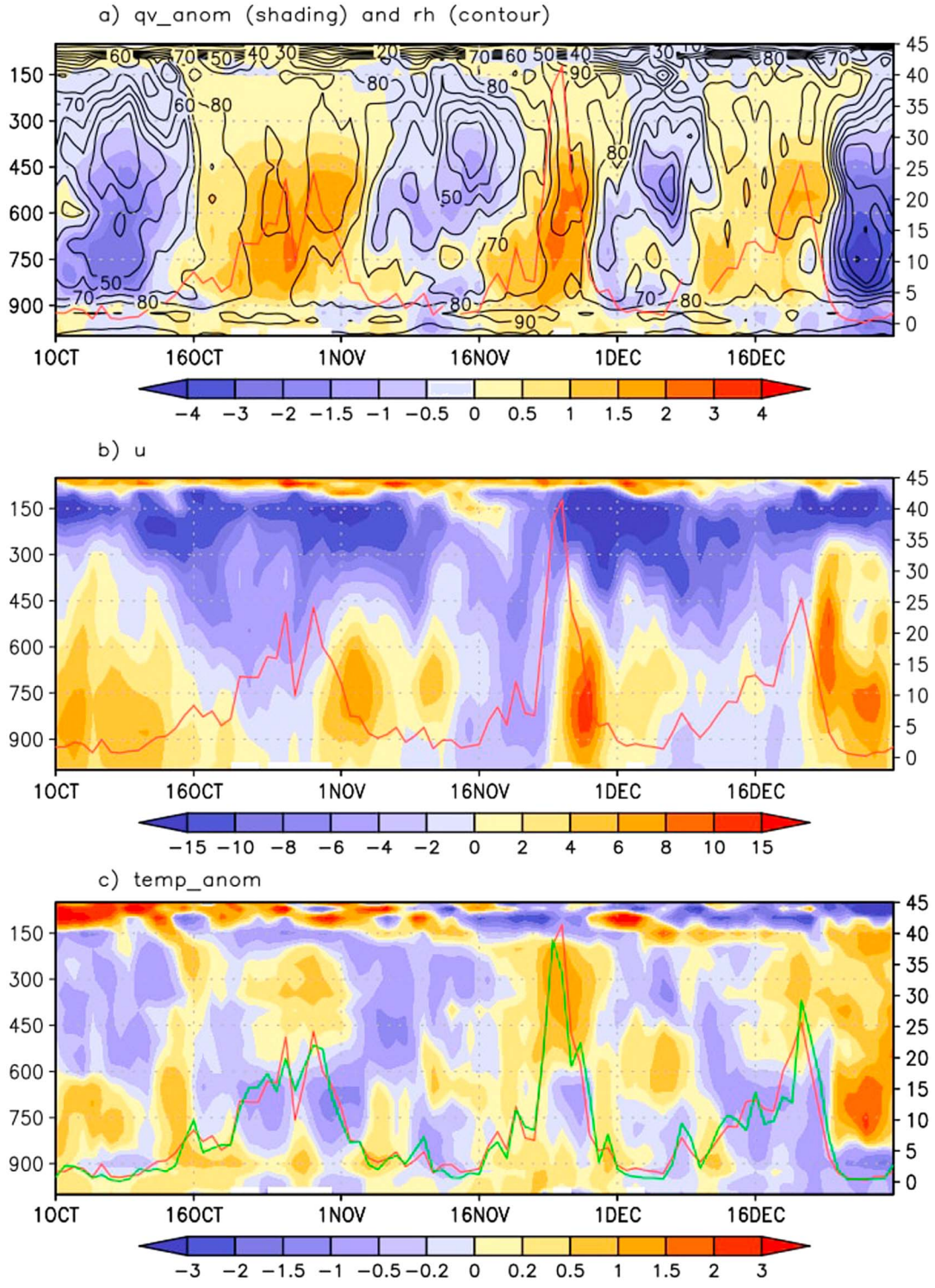

Figure 6. Vertical profiles of daily mean (a) relative humidity (contour, %) and specific humidity anomalies (shading, g kg^{-1}), (b) zonal wind (m s^{-1}), and (c) temperature anomalies (K) averaged over the NSA in the DYNAMO reanalysis. (The anomalies are obtained by removing the October–December 2011 mean from the daily mean fields.)The red line in all three panels is daily mean precipitation (mm d^{-1}) averaged over the NSA from the DYNAMO reanalysis, and the green line Figure 6c is the corresponding time series from TRMM 3B42 data. Both precipitation time series are plotted against right *Y* axis. Left *Y* axis is pressure in hectopascals and *X* axis is time in days from 1 October to 31 December 2011.

Figure 5 shows the effective gain, contextual bias, and correlation between O-F and A-F for the DYNAMO soundings over the NSA for 1 October 2011 to 31 December 2011, as a function of vertical pressure levels. The effective gain for the winds indicates that the corrections are primarily below 100 hPa, where linear regression coefficient between the O-F and A-F is as high as 0.6–0.7 with about 0.9 correlation between O-F and A-F. The contextual bias is near-zero for zonal and meridional winds. For temperature and specific humidity, the regression coefficient is 0.4–0.5 for levels 900–300 hPa, with correlations at or greater than 0.8. Above 200 hPa, the effective gain and correlation decrease sharply as the data count decreases. Comparing temperature and specific humidity, the contextual bias is close to zero for temperature at all pressure levels, and for specific humidity above 600 hPa. The contextual bias for specific humidity is about -0.2 for 1000–600 hPa indicating potential disagreement between DYNAMO soundings and radiance data. This may be due to the influence of moisture sources below 600 hPa such as AIRS, IASI, and microwave humidity sensors that are on board various satellites.

Results were also produced for a larger tropical Indian Ocean (TIO, 60°E–120°E, 15°S–15°N) region, and found to be generally similar to those in Figures 3–5 (not shown), suggesting the features discussed above are largely uniform in the entire DYNAMO region.

The above discussion suggests that the DYNAMO observations have a strong impact on the GMAO reanalysis basic fields, where they help to reduce model biases such as dry and cold biases in the lower troposphere and warm bias in the upper troposphere, along with considerable corrections in the horizontal winds.

4. Representation of the MJO Initiation Over Tropical Indian Ocean

4.1. Vertical Profiles of Zonal Wind, Temperature, and Humidity

Figure 6 shows the time series of daily mean specific humidity and air temperature anomalies, relative humidity, zonal wind, and precipitation from the DYNAMO reanalysis averaged over the NSA. The anomalies are obtained by removing the October–December 2011 mean from the daily mean fields. The DYNAMO reanalysis reproduces the three convective events in October, November, and December, as seen in the relative humidity and rainfall maxima in those months. The convective events that occurred during October and November are classified as having moderate amplitude with eastward propagation features (MJO-1 and MJO-2, hereafter), whereas the third event in December has less coherent propagation [*Johnson and Ciesielski*, 2013] and is not classified as a MJO. Based on the NSA-averaged moisture budget of the DYNAMO sounding based data, *Ruppert and Johnson* [2015] distinguished three subdivisions during the two DYNAMO MJO events, namely, suppressed (1–13 October and 10–16 November), bottom-heavy convective heating (14–19 October and 17–21 November, here we refer to this as preonset) and top-heavy convective heating (20 October to 4 November and 22–30 November or the deep convective phase as referred to in this study). We follow this classification in the rest of the paper. The evolution of the rainfall in the DYNAMO reanalysis agrees well with the observed TRMM 3B42 data [*Huffman et al*., 2007], capturing in particular the double rainfall peaks during MJO-1 (Figure 6c). A wet atmospheric column with relative humidity $>70\%$ is seen around 16 October to 2 November during MJO-1 and again around 16–30 November during MJO-2, approximately matching the peak convective phases. These are preceded and followed by very dry conditions (relative humidity $< 40\%$) indicative of suppressed phases. A total column drying is seen before MJO-1 with dry conditions reaching down to 850 hPa, whereas the dry conditions reach only up to 550 hPa during MJO-2. The stronger drying prior to MJO-1 can be partly due to the persistent westerly wind observed in the low-middle troposphere (from surface to approximately 450 hPa), which is typically drier relative to the moisture-laden easterlies from the warm pool, as well as due to stronger descending motion observed prior to MJO-1 (figure not shown). The gradual low-level moistening and associated tilted vertical profiles of moisture are evident in the specific humidity anomalies (Figure 6a), beginning around 15 October and 16 November, during MJO-1 and MJO-2, respectively.

The zonal wind over the NSA is characterized by weak low-level easterlies during the peak convective phase of the two MJO events, followed by strong low-level westerlies during the suppressed periods, again, in agreement with the sounding data. The low-level westerlies facilitate the influx of dry air form the western Indian Ocean resulting in a rather abrupt drying of the atmospheric column, setting up the suppressed MJO phase. Another feature noted in the sounding observations is the tilting of the temperature anomalies that facilitates the decent of cold anomalies in the upper troposphere, above 200 hPa [*Johnson and Ciesielski*,

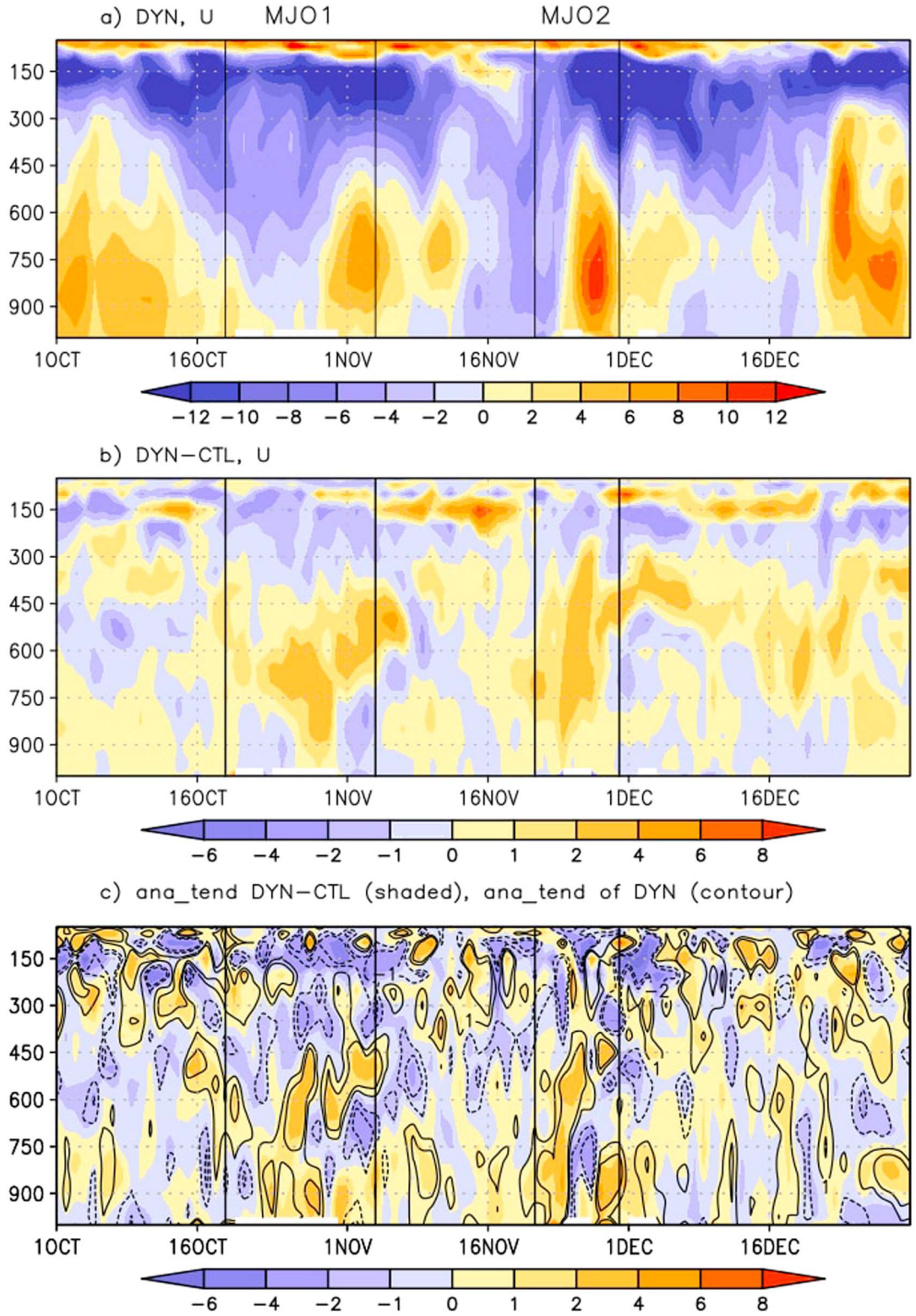

Figure 7. Vertical profiles of daily mean (a) zonal wind in the DYNAMO reanalysis (m s^{-1}), (same as in Figure 6b but reproduced here for easy comparison), (b) difference between the control and the DYNAMO reanalyses (m s^{-1}), and the (c) difference in zonal wind analysis tendency term (shading) and zonal wind analysis tendency term in the DYNAMO reanalysis (contour, m s^{-1} d^{-1}), all averaged over the NSA. *Y* axis is pressure in hectopascals, and *X* axis is time in days from 1 October to 31 December 2011. Vertical lines represent duration of MJO-1 and MJO-2, as labeled in Figure 7a.

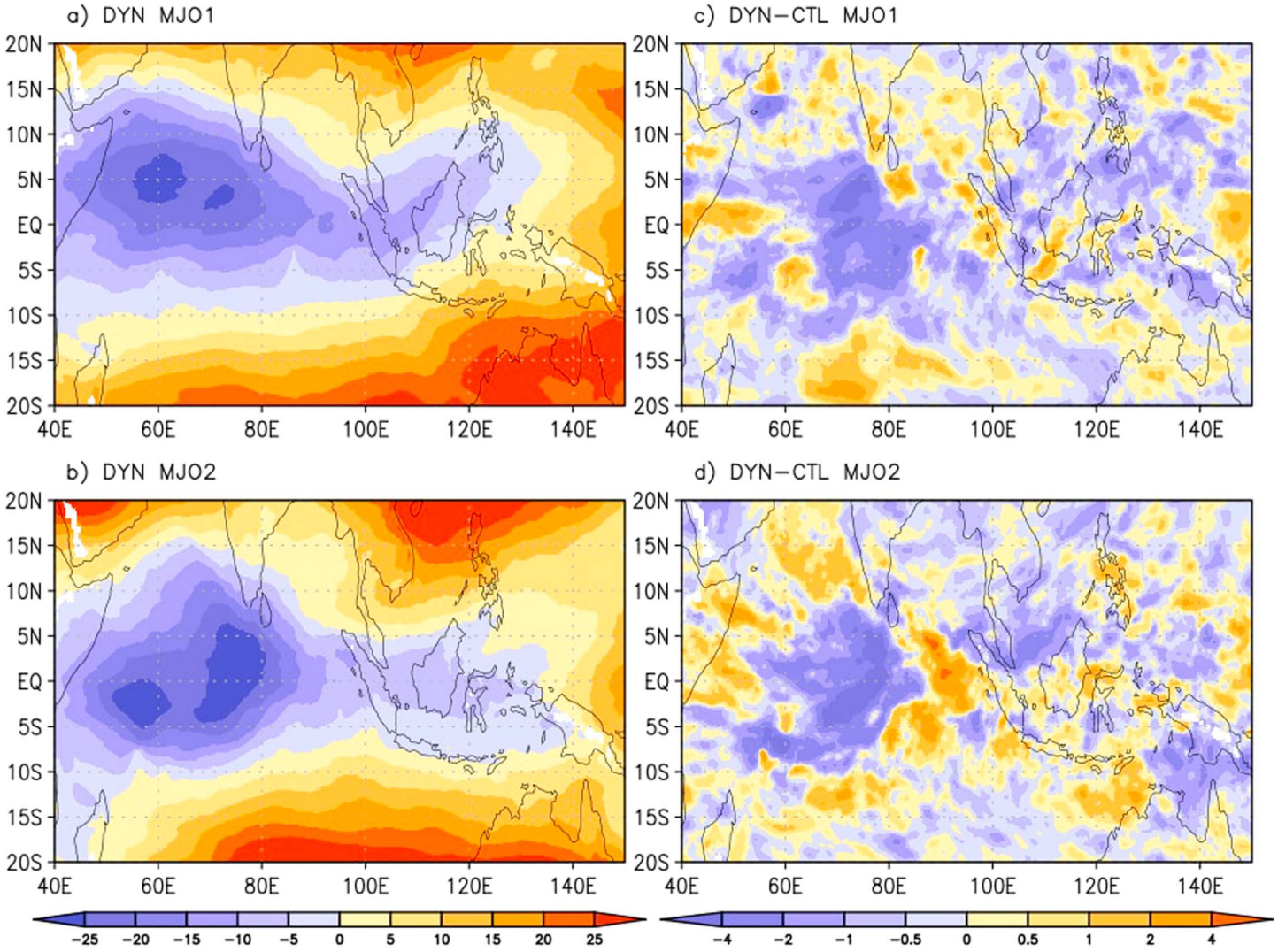

Figure 8. Zonal wind shear ($U_{200\,hPa}$–$U_{850\,hPa}$) (m s^{-1}) in the DYNAMO reanalysis averaged during (a) MJO-1 and (b) MJO-2 and (c and d) their corresponding difference fields from the control reanalysis. The averaging period is 29 October to 7 November for MJO-1 and 24–30 November for MJO-2, roughly corresponding to the mature phases of the MJO events.

2013]. This feature, which was most evident during MJO-2, is reproduced in the DYNAMO reanalysis (Figure 6c). Overall, the above results indicate that the MJO events in the DYNAMO reanalysis are in agreement with the sounding based profiles discussed in *Johnson and Ciesielski* [2013] and *Ruppert and Johnson* [2015].

Results from the array averaged sounding data have shown that the MJO signal was more predominant over the NSA than the southern sounding array (SSA), which consisted of 4 stations located at or south of the equator, namely, Diego Garcia, Gan, and the research vessels, Mirai and Revelle. In agreement with the observations, we noticed that the moisture profiles and precipitation time series in the DYNAMO reanalysis when averaged over the DYNAMO SSA (70°E–85°E, 9°S–0°), showed less distinct maxima during the MJO peak phases (figure not shown). This is in agreement with the observation by *Johnson and Ciesielski* [2013] that the SSA captured a continuous precipitation event associated with the tropical convergence zone, as opposed to the discrete, organized convective events, MJO-1 and MJO-2, observed at the NSA.

Figure 7 depicts the differences in zonal wind over the NSA between the DYNAMO and the control reanalyses. During the onset phases of the two MJO events, relative to the control reanalysis, the DYNAMO reanalysis shows weaker low-level easterlies and stronger upper level easterlies. Prior to, and following the convective peaks, the low-middle level westerlies are enhanced in the DYNAMO by 2–4 m s^{-1}, along with

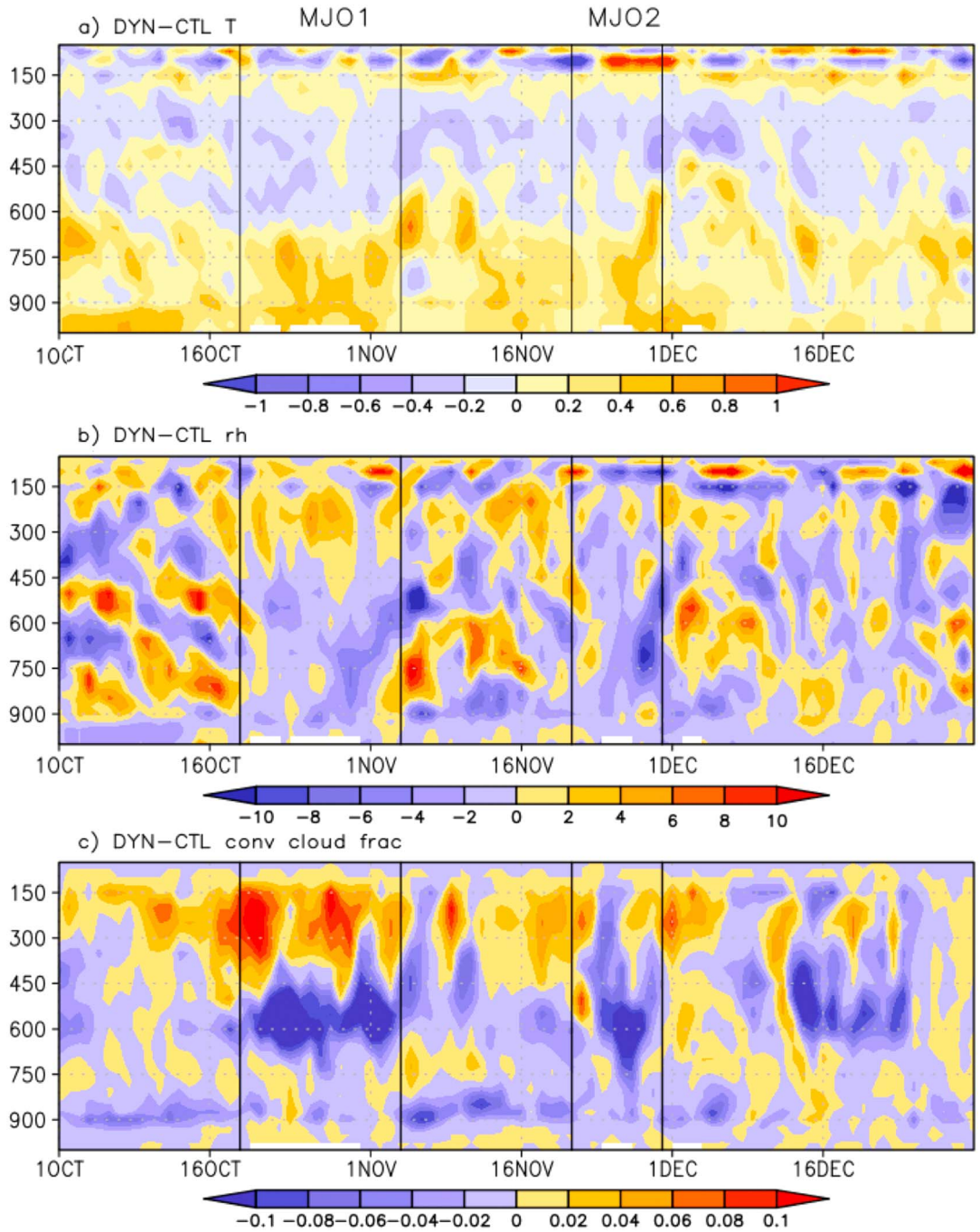

Figure 9. Difference between the DYNAMO and control reanalyses for (a) air temperature (K) and (b) relative humidity (%) and (c) convective cloud fraction (fraction), averaged over the NSA. *Y* axis is pressure in hectopascals and *X* axis is time in days from 1 October to 31 December 2011. Vertical lines represent duration of MJO-1 and MJO-2, as labeled in Figure 9a.

a slight increase in upper level easterlies between 300 and 150 hPa, suggesting an enhanced baroclinic structure of the MJO. The observations' effect on the reanalysis should also be seen in the analysis tendency term. This is the time tendency term that carries the observational information, which is added to the model prognostic equations as part of the IAU procedure in the GMAO assimilation system. Figure 7c shows the difference in the zonal wind analysis tendency term between the DYNAMO and control reanalyses, which is largely in agreement with Figure 7b, indicating that the improvements are directly due to the assimilation of DYNAMO observations. For clarity, Figure 7c also shows the zonal wind analysis tendency term of the

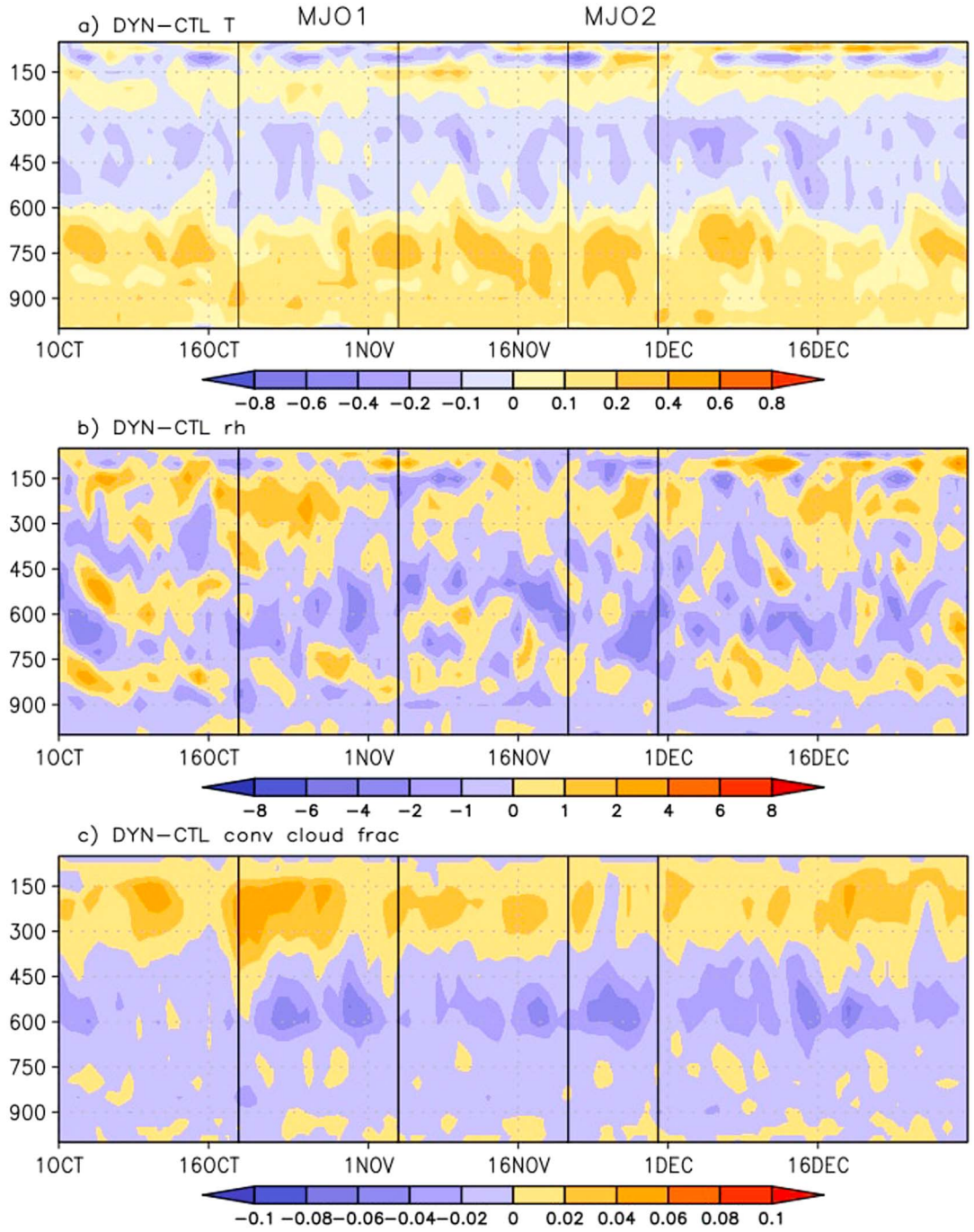

Figure 10. Same as in Figure 9 but for TIO domain.

DYNAMO reanalysis (contours), which has similar patterns as in the difference in analysis tendency terms (shading). The enhanced baroclinic structure is further evident in Figure 8, where the vertical zonal wind shear fields averaged over the trailing end of the two MJOs are shown. The vertical wind shear is computed as $U_{200\,\mathrm{hPa}}$–$U_{850\,\mathrm{hPa}}$ and is averaged over 29 October to 7 November (MJO-1) and 24–30 November (MJO-2), roughly corresponding to the peak convective phases of the two events. As inferred from the time series difference plot (Figure 7b), the difference maps of the wind shear indicate somewhat stronger shear in the DYNAMO reanalysis over the NSA domain.

Figure 9 shows vertical profiles of air temperature, relative humidity, and convective cloud area fraction averaged over the NSA. The cloud fraction is a prognostic variable calculated in the Relaxed Arakawa Schubert scheme of the GEOS-5 model based on the convective mass flux estimates [*Moorthi and Suarez*, 1992; *Bacmeister et al*., 2006]. In agreement with the inferences from the O-F and O-A profiles in Figure 3, the DYNAMO reanalysis is warmer in the lower troposphere and cooler in the upper troposphere than the control reanalysis, thereby reducing the lower tropospheric cold bias and upper tropospheric warm bias in the assimilating model. The lower troposphere, from surface to 600 hPa, is warmer by 0.2–0.5° in the DYNAMO reanalysis. The relative humidity profiles show an increase in moisture in the lower troposphere, particularly notable prior to the onset of MJO-1. The warmer lower troposphere aids in deep convection, which is seen in the enhanced convective cloud fraction in Figure 9c. Consistent with the enhanced convective cloud fraction, the upper level relative humidity shows an increase.

As mentioned in section 3, the impact of the DYNAMO observations is largely uniform in the entire DYNAMO region. This is further illustrated here by examining the difference plots over the TIO region (Figure 10). Comparing Figures 9 and 10, the temperature, moisture, and convective cloud fraction follow the profiles of the NSA, although the differences are relatively smaller due to the larger averaging domain.

4.2. Vertical Profile of Diabatic Heating and Low-Level Moisture Anomalies

There is a general consensus that the MJO deep convective (or the onset) phase is preceded by a preonset phase, where shallow convection and the low-level diabatic heating precondition the atmosphere for the deep convection [*Bladé and Hartmann*, 1993; *Hu and Randall*, 1994; *Benedict and Randall*, 2009; *Maloney*, 2009; *Kikuchi and Takayabu*, 2004, among others]. This was also one of the scientific rationales behind the DYNAMO field campaign [*Yoneyama et al*., 2013]. During the preonset phase, cloud population gradually develops from shallow cumuli to cumulus congestus, moisture builds up in the lower troposphere, and the sea surface temperature increases, setting up a convectively unstable atmospheric column and eventually triggering deep convection. Two processes thought to be critical to the low-level moistening are the detrainment from shallow clouds [*Johnson et al*., 1999; *Kikuchi and Takayabu*, 2004] and horizontal moisture advection [*Benedict and Randall*, 2009; *Maloney*, 2009]. During the onset or the deep convective phase, the sea surface cools due to cloud radiative effects and enhanced upper ocean mixing and air-sea fluxes, and the peak in moisture and the diabatic heating profiles shift upward, resulting in total column moistening and heating. For the DYNAMO MJO events, a number of studies examined the above mentioned mechanisms, for example, the moisture buildup by *Johnson and Ciesielski* [2013] and *Powell and Houze* [2015], detrainment from shallow clouds by *Hagos et al.* [2014], and horizontal moisture advection by *Sobel et al.* [2014]; *Tseng et al.* [2015] and *Nasuno et al.* [2015].

In this section, we show that relative to the control reanalysis, the DYNAMO reanalysis provides an improved representation of the vertical profile of diabatic heating and associated processes, in both the MJO preonset phase and deep convective phases. To illustrate this, we show results of precipitation rate binning analysis (similar to the diagnostic presented in *Klingaman et al.* [2015] and references therein) performed on relevant quantities. The compositing or binning is performed for a total of 22 precipitation rate bins (from 2-D precipitation fields) for 3-D fields over the NSA for daily mean values from 1 October to 31 December 2011. The bin intervals are selected accounting for the inherent nonlinearity of the precipitation data and are similar to the TRMM-based intervals used by *Klingaman et al.* [2015], except that we have used slightly finer intervals for medium to very high precipitation rates. Adopting the MJO phases from *Ruppert and Johnson* [2015] (see section 4.1) and examining the precipitation probability distributions during the calendar days specified above, we find that the grid point precipitation rates are generally less than 1 mm d^{-1} during the suppressed phase, although isolated values as high as 3–4 mm d^{-1} were observed at times. During the bottom-heavy convective phase, the precipitation rates range between 2 and 10 mm d^{-1}, and during the top-heavy convection, they mostly fall between 2–20 mm d^{-1}, with occasional high values reaching above 100 mm d^{-1}.

The daily diabatic heating (or apparent heating, Q1) is computed as a residual in the thermodynamic equation in pressure coordinates, using daily reanalysis outputs [*Yanai et al*., 1973; *Yanai and Tomita*, 1998]. This approach has been commonly used to obtain apparent heating from reanalysis temperature and circulation fields. Such derived diabatic heating incorporates the effects of the analysis increments and is considered to better agree with the reanalysis circulation fields than the standard reanalysis heating output. For both the control and the DYNAMO reanalyses, daily mean fields of the diabatic heating are produced for 42 pressure

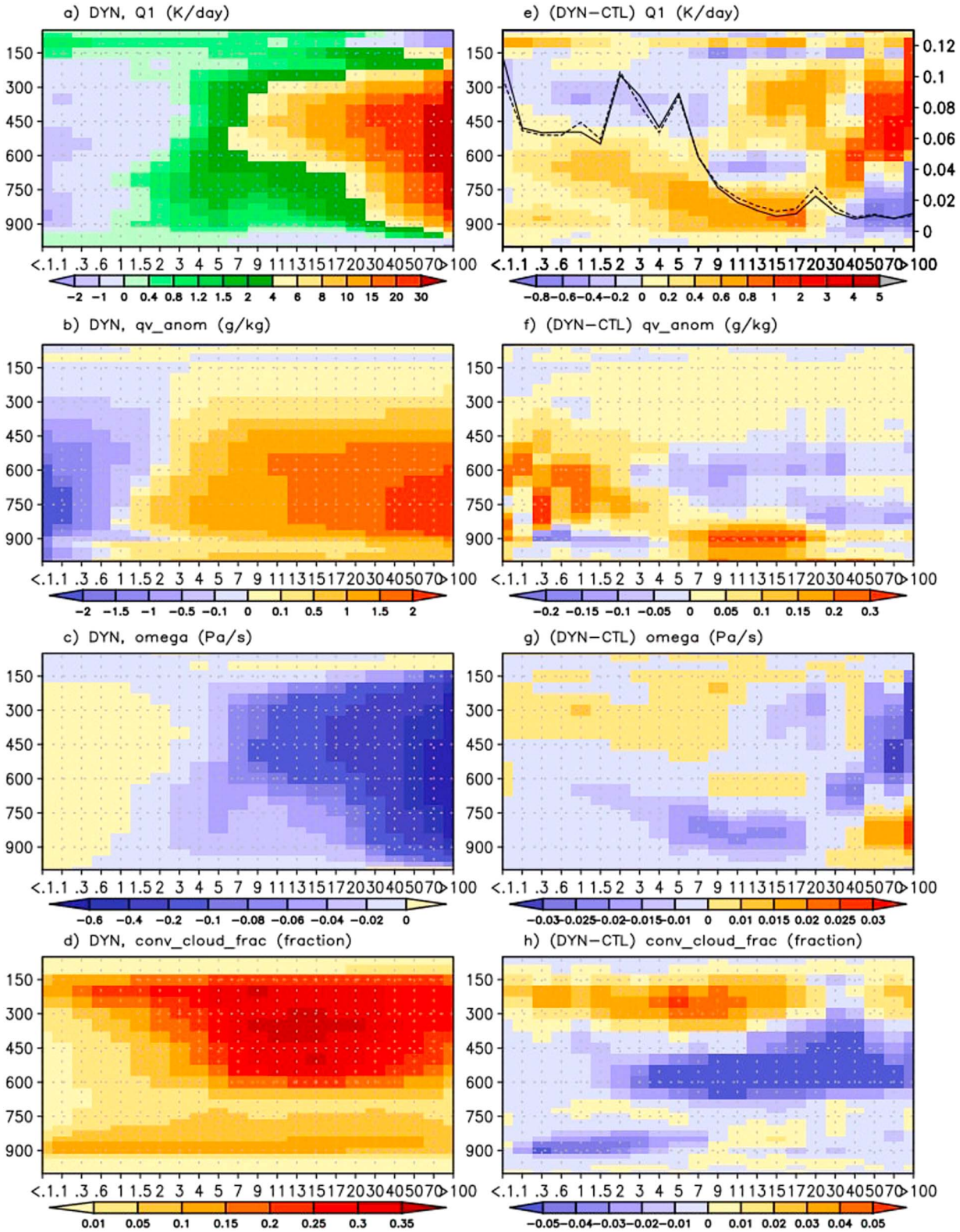

Figure 11. Composite vertical profiles with respect to precipitation rate bins for (a) derived diabatic heating (Q1, K^{-1}), (b) specific humidity anomalies (g kg^{-1}), (c) vertical pressure velocity (Pa s^{-1}), and (d) convective cloud fraction (fraction). (The anomalies are obtained by removing the October–December 2011 mean from the daily mean fields.) (e–h) Their corresponding difference from the control reanalysis. The *X* axis is precipitation rate bins (mm d^{-1}) and *Y* axis is pressure (hPa). The composites are obtained by averaging the grid point quantities in the NSA domain for daily mean data from 1 October to 31 December 2011. The black lines in Figure 11e, plotted against the right *Y* axis, is the fraction of grid points averaged in each precipitation bin for the control (solid) and the DYNAMO (dotted) reanalyses.

levels. The Q1 fields of our reanalyses are qualitatively similar to the apparent heating derived from the 1° gridded DYNAMO observations from the sounding network [*Johnson and Ciesielski,* 2013; *Ciesielski et al*., 2014; *Johnson et al*., 2015] (not shown). However, a direct comparison with that data may not be fair, mainly due to the difference in horizontal resolutions between the two data sets.

Figures 11a–11d show the composite vertical profiles of the diabatic heating, specific humidity anomalies, vertical pressure velocity, and convective cloud fraction in the DYNAMO reanalysis, plotted as a function of precipitation rate. As in earlier cases, the anomalies are obtained by removing the October–December 2011 mean from the daily mean fields. The corresponding difference between the DYNAMO and the control reanalyses is shown in Figures 11e–11h. The number of grid points averaged in each precipitation bin is plotted along the right *Y* axis in Figure 11e, which shows that the sample size distribution is similar between the two reanalyses. Therefore, any difference shown in Figures 11e–11h is not due to difference in sample size between the two reanalyses.

In agreement with the generally accepted notion of the MJO initiation, a stepwise progression in heating and low-level moistening in connection with the transition from shallow cumulus to congestus to deep convection was observed in the DYNAMO sounding based moisture and diabatic heating profiles [*Johnson et al*., 2015; *Ruppert and Johnson*, 2015]. We find that this feature is better represented in the DYNAMO reanalysis, relative to the control reanalysis.

The composite profile of diabatic heating provides a picture that is largely consistent with the generally agreed upon notion of the evolution of the heating during the MJO (Figure 11a). The heating is predominantly in the lower levels (below 700 hPa) for low-medium rain rates (1–5 mm d^{-1}) and becomes elevated in the column as the precipitation rate increases to 5–20 mm d^{-1}. For intense rainfall rates (>20 mm d^{-1}), a composite total column heating of about 20–30 K d^{-1} is observed. Although this behavior is grossly similar in both the control and the DYNAMO reanalyses, there are notable differences between the two. The difference plot (Figure 11e) shows an enhanced heating of 0.2–0.8 K d^{-1} in the DYNAMO reanalysis in the lower troposphere for low-medium rain rates, indicative of enhanced low-level heating mostly during the MJO preonset phase. For precipitation rates 9–20 mm d^{-1}, the increase is nearly through the entire atmospheric column, reaching up to 200 hPa suggesting an overall enhancement of convection. An exception to this total column increase is found around 750 hPa, where the heating is slightly reduced in the DYNAMO reanalysis. (This point is further examined in section 5). For very intense precipitation rates (>40 mm d^{-1}), the heating profile is modified such that heating is greater in the middle-upper troposphere (above 600 hPa) whereas it is slightly reduced in the lower troposphere. However, we note that this feature is limited to a rather small sample size where the number of grid points with precipitation rate greater than 40 mm d^{-1} accounts for barely 1% of the total sample size.

The evolution of moisture anomalies with respect to precipitation rate (Figure 11b) shows a gradual bottom-up moistening starting from a precipitation rate of about 1 mm d^{-1}, which is similar to the ECMWF-TRMM composites of *Klingaman et al.* [2015]. For precipitation rates less than 1 mm d^{-1} the column is anomalously dry. As the precipitation rate reaches 3–4 mm d^{-1}, the entire column becomes anomalously moist, which is again similar to the behavior seen in the ECMWF-TRMM composites. In many current models, a sharp transition from dry to wet anomalies occurs, where the total column remains dry for precipitation rates as high as 2 mm d^{-1} and abruptly becomes wet when precipitation increases to 4 mm d^{-1}. While the GEOS-5 general circulation model is not immune to this behavior, here in the reanalysis framework, we find that a gradual transition occurs from dry column to wet column as the precipitation increases from 0.6 to 3 mm d^{-1}. The difference plot of the specific humidity profile shows enhanced low-level moisture for moderate precipitation rates of 7–17 mm d^{-1}, indicating an improved representation of low-level moisture during the preonset phase of the MJO. Another difference is in connection with the mid-tropospheric drying for rain rates less than 1 mm d^{-1}, where the dry anomalies are slightly reduced in the DYNAMO reanalysis, in comparison to the control reanalysis.

Similar to the diabatic heating and moisture anomalies, the composite profile of vertical velocity also indicates a distinct low-level strengthening of upward motion for moderate rain rates in the DYNAMO reanalysis. Additionally, for high precipitation rates, stronger upward vertical velocity is seen in the middle-upper troposphere in connection with the enhanced diabatic heating there and weaker upward velocity in the lower

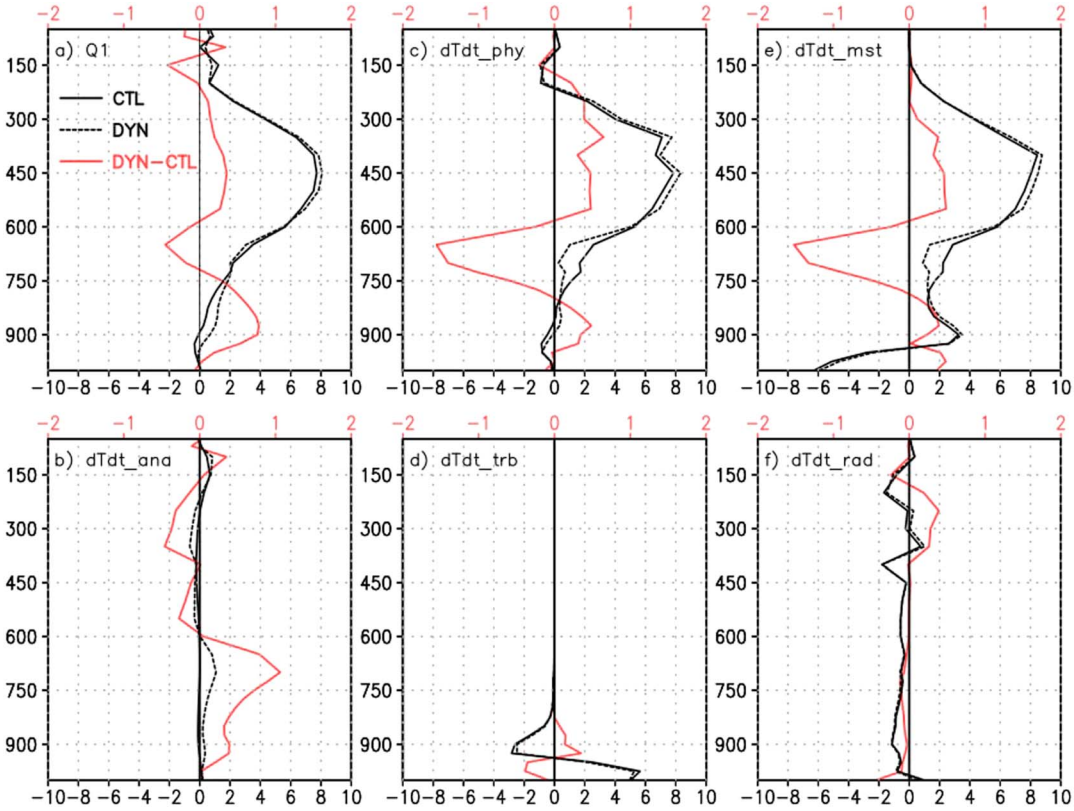

Figure 12. Composite vertical profile of the (a) derived diabatic heating (Q1) for the precipitation rate bin 11-13 mm d^{-1} for (black solid) the control reanalysis, (black dotted) DYNAMO reanalysis and (red, along top *Y* axis) the difference between them, and similar temperature tendency profiles for (b) analysis increment, (c) total physical processes, (d) turbulence, (e) moist processes, and (f) radiation. Units are in K d^{-1}. *Y* axis is pressure in hectopascals.

troposphere corresponding to the decrease in heating there. The enhanced convective activity that is implied in the diabatic heating profiles is further evident in the convective cloud fraction profiles.

5. Relevance of Model Physics

The improvements discussed in section 4 can be considered as the combined result of the model's response to the observations (improvements in the model background) and the direct corrections from the observations through analysis tendency terms. However, the model physics plays a crucial role in shaping the final reanalysis outputs, especially for regions and periods where the convective processes are critical. Here we describe such an instance where the model physics appears to have problems in fully integrating the DYNAMO observations.

The decrease in diabatic heating between 600 and 700 hPa when model precipitation ranges from 9 to 17 mm d^{-1} in the DYNAMO reanalysis in Figure 11e (mentioned above) appears to stem from a poor model background. In Figure 12, we focus on a single precipitation rate bin (11–13 mm d^{-1}) that is representative of the above mentioned range and examine the composites of the individual components of the reanalysis heating (moist physics that mainly account for cloud-related processes, turbulence, and radiation) along with the temperature analysis tendency term. Figure 12 shows that the small decrease in Q1 (~0.4 K d^{-1}) between 700 hPa and 600 hPa is mainly the result of a considerable decrease (about 1–2 K d^{-1}) in the heating due to moist processes (Figures 12a, 12c, and 12e). Although it is partially offset by an increase from the analysis tendency term (1 K d^{-1}), the total heating (Q1) is left with a small decrease, in comparison to the control reanalysis. The turbulence and the radiative components are similar between the two reanalyses and do not contribute to the above mentioned difference.

This model behavior is reminiscent of the finding of *Mapes and Bacmeister* [2012], where they pointed out a sharp cooling bias around 700 hPa in an early version of the GEOS-5 AGCM by examining the MERRA analysis

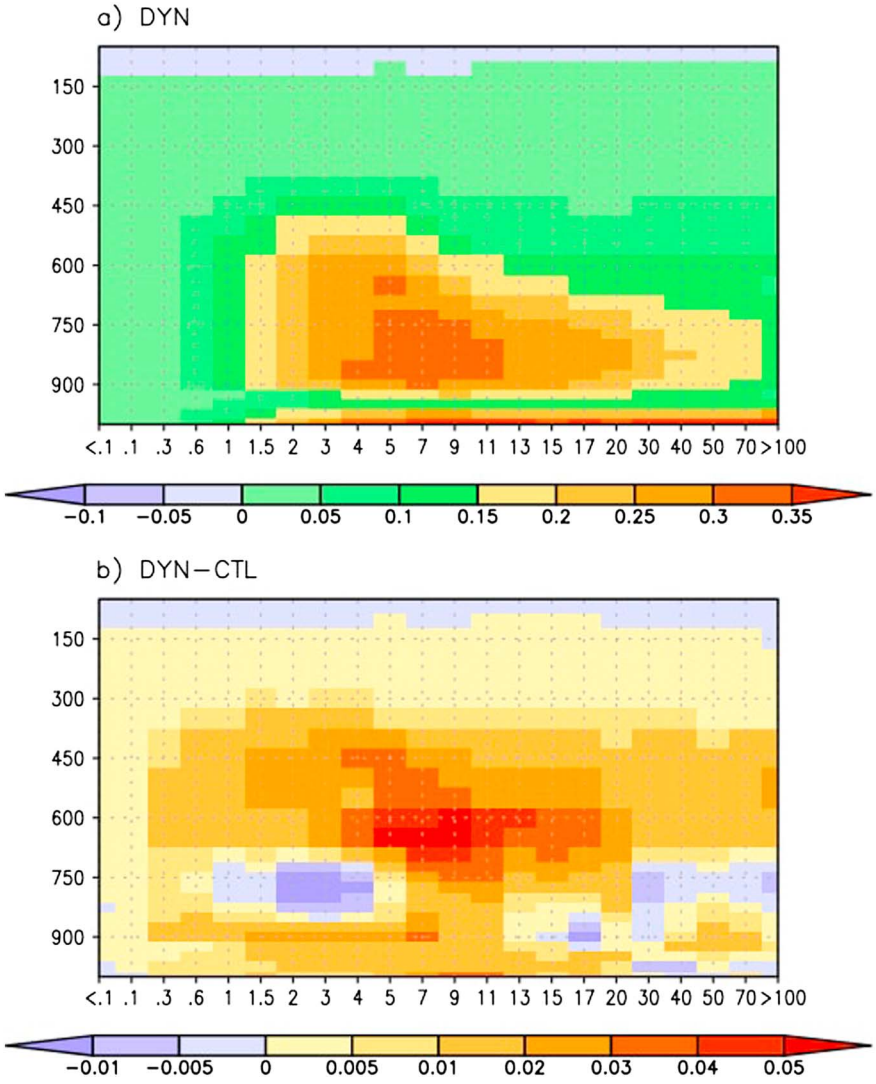

Figure 13. Composite vertical profiles with respect to precipitation rate bins for evaporation of convective precipitation (g kg^{-1} d^{-1}) for (a) DYNAMO reanalysis and (b) the corresponding difference from the control reanalysis. The *X* axis is precipitation rate bins (mm d^{-1}), and *Y* axis is pressure (hPa). The composites are obtained as in Figure 8, by averaging the grid point quantities in the NSA domain for daily mean data from 1 October to 31 December 2011.

tendency terms. They noticed that the model's moist physics had excessive re-evaporation and erroneous sharp cooling at 700 hPa. A similar model bias is likely acting in the current GEOS-5 AGCM as well, which is interestingly enhanced when the model is subject to the influence of the DYNAMO observations. Composite vertical profiles of the model's re-evaporation of convective rain (Figure 13) shows that an enhanced re-evaporation is present in the DYNAMO reanalysis, between 750 and 450 hPa, for precipitation rates 4–17 mm d^{-1}, which is possibly responsible for the sharp decrease in physical heating. The increase in re-evaporation is particularly distinct between 600 and 750 hPa. As noted in the convective cloud fraction profiles in Figure 11h, the convection is invigorated in the DYNAMO reanalysis, resulting in enhanced re-evaporation of the convective rain, which in turn produces the decrease in heating.

6. Summary and Discussion

This study investigates the impact of the DYNAMO observations on the quality of GMAO reanalyses with a focus on the representation of the MJO initiation processes over the central tropical Indian Ocean. For the investigation, we produced a high-resolution global reanalysis by assimilating quality-controlled, high vertical resolution DYNAMO upper air soundings, using essentially the same version

of the NASA GMAO atmospheric data assimilation system that is being used for the newly released MERRA-2 reanalysis, though run at somewhat higher horizontal resolution. In order to cleanly assess the impact of the DYNAMO observations, a companion control reanalysis was produced where the DYNAMO data were withheld and the DYNAMO GTS submissions were removed from the conventional data buffer.

The assimilation of the DYNAMO observations improves the reanalysis in many respects. The vertical structure of reanalysis temperature, humidity, and zonal winds over the DYNAMO region are more realistic in the DYNAMO reanalysis than in the control reanalysis. Biases in the assimilating model over the central tropical Indian Ocean, such as the cold and dry biases in the lower troposphere and warm bias in the upper troposphere, are further reduced in the DYNAMO reanalysis. In general, relative to the control reanalysis, the DYNAMO reanalysis has a warmer and moister lower troposphere and cooler upper troposphere. The zonal winds in the DYNAMO reanalysis exhibit stronger low-middle level westerlies, in better agreement with the observed westerly acceleration during the winding down of the October and November MJO events, and enhancing their baroclinic structure. In connection with the MJO initiation, the assimilation of DYNAMO observations increases low-level moisture anomalies and diabatic heating during the preonset phase of the MJO. During the deep convective phase, the deep convection is stronger in the DYNAMO reanalysis as indicated by the enhancement of the diabatic heating, vertical pressure velocity, and convective cloud fraction, in the middle and upper troposphere.

Although the DYNAMO observations tend to improve the reanalysis in general, biases in the assimilating model can be problematic unless they are fully corrected by the analysis tendency terms. Despite the overall improvements in the low-level diabatic heating for low-medium precipitation rates, the model response above 700 hPa appears to be in disagreement with the observations where a sharp decrease in the total heating was observed. This model bias is possibly connected to the excessive re-evaporation at that level, which is initiated by the invigorated convection in the DYNAMO reanalysis.

We note that the impact of DYNAMO observations on GMAO reanalysis varies with the spatial resolution of the analysis system, particularly with the resolution of the GEOS-5 AGCM. Results from parallel lower (1°) horizontal resolution DYNAMO and control reanalyses (not shown) show that the corrections from the DYNAMO observations are larger there, compared to the 1/4° experiments discussed here. This is because the higher-resolution GEOS-5 AGCM uses a stronger minimum threshold of entrainment by default, and is thus less affected by the biases from the GEOS-5 Relaxed Arakawa-Schubert Scheme; the GMAO reanalyses at higher resolution thus require smaller corrections from the DYNAMO observations.

While a reanalysis devoid of in situ observations in the tropical Indian Ocean would still produce somewhat realistic large-scale features of the MJO, our study underlines the crucial importance of assimilating DYNAMO-like in situ observations, if available, in current reanalyses in order to provide a more faithful representation of the observed physical processes associated with MJO initiation. This is particularly necessary as long as the assimilating models continue to be deficient in simulating observed moist physical processes in the tropical Indian Ocean.

Acknowledgments

This study has been supported by the NOAA Earth System Science (ESS) program. The authors thank the data assimilation and modeling groups at the Global Modeling and Assimilation Office (GMAO) at the Goddard Space Flight Center (GSFC) for guidance in conducting the assimilation experiments. The assimilation runs are produced using the High-End Computing (HEC) platforms of the NASA Center for Climate Simulation (NCCS) at the GSFC. The DYNAMO and other data used in this study are listed in the references. The reanalyses data produced in this study are archived at the NCCS at the GSFC and are available from the authors upon request.

References

Bacmeister, J. T., M. J. Suarez, and F. R. Robertson (2006), Rain re-evaporation, boundary layer-convection interactions, and Pacific rainfall patterns in an AGCM, *J. Atmos. Sci.*, *63*, 3383–3403.

Benedict, J., and D. A. Randall (2009), Structure of the Madden–Julian oscillation in the super parameterized CAM, *J. Atmos. Sci.*, *66*, 3277–3296.

Bladé, I., and D. L. Hartmann (1993), Tropical intraseasonal oscillation in a simple nonlinear model, *J. Atmos. Sci.*, *50*, 2922–2939.

Bloom, S., L. Takacs, A. DaSilva, and D. Ledvina (1996), Data assimilation using incremental analysis updates, *Mon. Weather Rev.*, *24*, 1256–1271.

Bosilovich, M. G., and A. Da Silva (2013), Evaluation of the relative contribution of observing systems in reanalyses: Aircraft temperature bias and analysis innovations, paper presented at American Geophysical Union, Fall Meeting, San Francisco, Calif.

Bosilovich, M. G., et al. (2015), MERRA-2: Initial evaluation of the climate, *NASA/TM–2015-104606/Vol. 43*, NASA Goddard Space Flight Center, Greenbelt, Md.

Ciesielski, P. E., et al. (2014), Quality-controlled upper-air sounding dataset for DYNAMO/CINDY/AMIE: Development and corrections, *J. Atmos. Oceanic Technol.*, *31*, 741–764.

Donlon, C. J., M. Martin, J. Stark, J. Roberts-Jones, E. Fiedler, and W. Wimmer (2012), The Operational Sea Surface Temperature and Sea Ice Analysis (OSTIA) system, *Remote Sens. Environ.*, *116*, 140–158, doi:10.1016/j.rse.2010.10.017.

Gelaro, R., R. H. Langland, S. Pellerin, and R. Todling (2010), The THORPEX observation impact intercomparison experiment, *Mon. Weather Rev.*, *138*, 4009–4025.

Helfand, H. M., and S. D. Schubert (1995), Climatology of the simulated Great Plains low-level jet and its contribution to the continental moisture budget of the United States, *J. Clim.*, *8*, 784–806.
Hagos, S., Z. Feng, K. Landu, and C. N. Long (2014), Advection, moistening, and shallow-to-deep convection transitions during the initiation and propagation of Madden-Julian Oscillation, *J. Adv. Model. Earth Syst.*, *6*, 938–949, doi:10.1002/2014MS000335.
Hu, Q., and D. A. Randall (1994), Low-frequency oscillations in radiative-convective systems, *J. Atmos. Sci.*, *51*, 1089–1099.
Huffman, G. J., R. F. Adler, D. T. Bolvin, G. Gu, E. J. Nelkin, K. P. Bowman, Y. Hong, E. F. Stocker, and D. B. Wolff (2007), The TRMM multi-satellite precipitation analysis: Quasi-global, multi-year, combined-sensor precipitation estimates at fine scale, *J. Hydrometeor.*, *8*, 38–55.
Hung, M.-P., J.-L. Lin, W. Wang, D. Kim, T. Shinoda, and S. J. Weaver (2013), MJO and convectively coupled equatorial waves simulated by CMIP5 climate models, *J. Clim.*, *26*, 6185–6214.
Jiang, X., D. E. Waliser, W. S. Olson, W.-K. Tao, T. S. L'Ecuyer, S. Shige, K.-F. Li, Y. L. Yung, S. Lang, and Y. N. Takayabu (2011), Vertical diabatic heating structure of the MJO: Intercomparison between recent reanalyses and TRMM estimates, *Mon. Weather Rev.*, *139*, 3208–3223.
Johnson, R. H., and P. E. Ciesielski (2013), Structure and properties of Madden–Julian Oscillations deduced from DYNAMO sounding arrays, *J. Atmos. Sci.*, *70*, 3157–3179.
Johnson, R. H., T. M. Rickenbach, S. A. Rutledge, P. E. Ciesielski, and W. H. Schubert (1999), Trimodal characteristics of tropical convection, *J. Clim.*, *12*, 2397–2418.
Johnson, R. H., P. E. Ciesielski, J. H. Ruppert Jr., and M. Katsumata (2015), Sounding-based thermodynamic budgets for DYNAMO, *J. Atmos. Sci.*, *72*, 598–622.
Kikuchi, K., and Y. N. Takayabu (2004), The development of organized convection associated with the MJO during TOGA COARE IOP: Trimodal characteristics, *Geophys. Res. Lett.*, *31*, L10101, doi:10.1029/2004GL019601.
Kim, H. M., C. D. Hoyos, P. J. Webster, and I. S. Kang (2010), Ocean– atmosphere coupling and the boreal winter MJO, *Clim. Dyn.*, *35*, 771–784.
Kleist, D. T., D. F. Parrish, J. C. Derber, R. Treadon, W.-S. Wu, and S. Lord (2009), Introduction of the GSI into the NCEPs Global Data Assimilation System, *Weather Forecast*, *24*, 1691–1705.
Klingaman, N. P., et al. (2015), Vertical structure and physical processes of the Madden-Julian oscillation: Linking hindcast fidelity to simulated diabatic heating and moistening, *J. Geophys. Res. Atmos.*, *120*, 4690–4717, doi:10.1002/2014JD022374.
Koster, R. D., M. J. Suárez, A. Ducharne, M. Stieglitz, and P. Kumar (2000), A catchment-based approach to modeling land surface processes in a GCM, Part 1: Model structure, *J. Geophys. Res.*, *105*, 24,809–24,822, doi:10.1029/2000JD900327.
Lin, J.-L., et al. (2006), Tropical intraseasonal variability in 14 IPCC AR4 climate models. Part I: Convective signals, *J. Clim.*, *19*, 2665–2690.
Lin, S. J. (2004), A vertically Lagrangian finite-volume dynamical core for global models, *Mon. Weather Rev.*, *132*, 2293–2307.
Ling, J., and C. Zhang (2011), Structural evolution in heating profiles of the MJO in global reanalyses and TRMM retrievals, *J. Clim.*, *24*, 825–842.
Ling, J., P. Bauer, P. Bechtold, A. Beljaars, R. Forbes, F. Vitart, M. Ulate, and C. D. Zhang (2014), Global versus local MJO forecast skill of the ECMWF model during DYNAMO, *Mon. Weather Rev.*, *142*, 2228–2247.
Lock, A. P., A. R. Brown, M. R. Bush, G. M. Martin, and R. N. B. Smith (2000), A new boundary layer mixing scheme. Part I: Scheme description and single-column model tests, *Mon. Weather Rev.*, *138*, 3187–3199.
Louis, J. F., M. Tiedtke, and J-F. Geleyn (1982), A short history of the PBL parameterization at ECMWF, in *Workshop on Boundary-Layer Parametrizations*, pp. 59–79, ECMWF, Reading, U. K. [Available at http://www.ecmwf.int/publications/.]
Madden, R. A., and P. R. Julian (1971), Detection of a 40–50 day oscillation in the zonal wind in the tropical Pacific, *J. Atmos. Sci.*, *28*, 702–708.
Madden, R. A., and P. R. Julian (1972), Description of global-scale circulation cells in the tropics with a 40-50 day period, *J. Atmos. Sci.*, *29*, 1109–1123.
Maloney, E. D. (2009), The moist static energy budget of a composite tropical intraseasonal oscillation in a climate model, *J. Clim.*, *22*, 711–729.
Mapes, B. E., and J. T. Bacmeister (2012), Diagnosis of tropical biases and the MJO from patterns in the MERRA analysis tendency fields, *J. Clim.*, *25*, 6202–6214.
Molod, A., L. Takacs, M. Suarez, and J. Bacmeister (2015), Development of the GEOS-5 atmospheric general circulation model: evolution from MERRA to MERRA2, *Geosci. Model Dev.*, *8*, 1339–1356, doi:10.5194/gmd-8-1339-2015.
Moorthi, S., and M. J. Suarez (1992), Relaxed Arakawa Schubert: A parameterization of moist convection for general circulation models, *Mon. Weather Rev.*, *120*, 978–1002.
Nasuno, T., T. Li, and K. Kikuchi (2015), Moistening processes before the convective initiation of Madden-Julian Oscillation events during the CINDY2011/DYNAMO period, *Mon. Weather Rev.*, *143*, 622–643.
Powell, S. W., and R. A. Houze Jr. (2015), The effect of dry large-scale vertical motions on initial MJO convective onset, *J. Geophys. Res. Atmos.*, *120*, 4783–4805, doi:10.1002/2014JD022961.
Putman, W., and S.-J. Lin (2007), Finite volume transport on various cubed sphere grids, *J. Comput. Phys.*, *227*, 55–78, doi:10.1016/j.jcp.2007.07.022.
Rienecker, M. M., et al. (2008), *The GEOS-5 Data Assimilation System—Documentation of Versions 5.0.1, 5.1.0, and 5.2.0, NASA/TM–2008–104606*, NASA Goddard Space Flight Center, Greenbelt, Md.
Robertson, F. R., and J. B. Roberts (2012), Intraseasonal variability in MERRA energy fluxes over the tropical oceans, *J. Clim.*, *25*, 5629–5647, doi:10.1175/JCLI-D-11-00428.1.
Ruppert, R. H., Jr., and R. H. Johnson (2015), Diurnally modulated cumulus moistening in the preonset stage of the Madden–Julian Oscillation during DYNAMO, *J. Atmos. Sci.*, *72*, 1622–1647.
Seo, K. H., W. Q. Wang, J. Gottschalck, Q. Zhang, J. K. E. Schemm, W. R. Higgins, and A. Kumar (2009), Evaluation of MJO forecast skill from several statistical and dynamical forecast models, *J. Clim.*, *22*, 2372–2388.
Sobel, A., S. Wang, and D. Kim (2014), Moist static energy budget of the MJO during DYNAMO, *J. Atmos. Sci.*, *71*, 4276–4291.
Tseng, K. C., C. H. Sui, and T. Li (2015), Moistening processes for Madden-Julian Oscillation during DYNAMO/CINDY, *J. Clim.*, *28*, 3041–3057.
Waliser, D. E. (2011), Predictability and forecasting, in *Intraseasonal Variability of the Atmosphere-Ocean Climate System*, edited by W. K. M. Lau and D. E. Waliser, pp. 433–468, Springer, Berlin.
Wang, B. (2011), Theory, in *Intraseasonal variability of the Atmosphere-Ocean Climate System*, edited by W. K. M. Lau and D. E. Waliser, pp. 307–360, Springer, Berlin.
Wu, W.-S., R. J. Purser, and D. F. Parrish (2002), Three-dimensional variational analysis with spatially inhomogeneous covariances, *Mon. Weather Rev.*, *130*, 2905–2916.
Yanai, M., and T. Tomita (1998), Seasonal and interannual variability of atmospheric heat sources and moisture sinks as determined from NCEP–NCAR reanalysis, *J. Clim.*, *11*, 463–482.
Yanai, M., S. Esbensen, and J.-H. Chu (1973), Determination of bulk properties of tropical cloud clusters from large-scale heat and moisture budgets, *J. Atmos. Sci.*, *30*, 611–627.

Yoneyama, K., C. Zhang, and C. N. Long (2013), Tracking pulses of the Madden–Julian Oscillation, *Bull. Am. Meteorol. Soc.*, *94*, 1871–1891.
Zhang, C. (2005), Madden-Julian Oscillation, *Rev. Geophys.*, *43*, RG2003, doi:10.1029/2004RG000158.
Zhang, C., J. Gottschalck, E. D. Maloney, M. W. Moncrieff, F. Vitart, D. E. Waliser, B. Wang, and M. C. Wheeler (2013), Cracking the MJO nut, *Geophys. Res. Lett.*, *40*, 1223–1230, doi:10.1002/grl.50244.